PRIFYSGOL
BANGOR
UNIVERSITY

Seasonal variability in the source and composition of particulate matter in the depositional zone of Baltimore Canyon, U.S. Mid-Atlantic Bight

Prouty, N.G.; Mienis, F.; Campbell, P.; Roark, E.B.; Davies, Andrew; Robertson, Craig; Duineveld, G.C.A.; Ross, S.W.; Rhode, M.; Demopoulos, A.W.J.

Deep Sea Research I: Oceanographic Research Papers

Peer reviewed version

Cyswllt i'r cyhoeddiad / Link to publication

19. Sept. 2024

Seasonal variability in the source and composition of particulate matter in the depositional zone of Baltimore Canyon, U.S. Mid-Atlantic Bight

Prouty[1]*, N.G., Mienis[2], F., Campbell[1], P., Roark[4], E.B., Davies[5], A.J., Robertson[5], C.M., Duineveld[2], G., Ross[6], S.W., Rhode[7], M., Demopoulos[8], A.W.J.

Highlights

- Vertical transport and lateral transport across the continental margin were the dominant processes driving seasonal input of particulate matter
- *n*-alkane and sterol biomarker results combined with isotopes and trace metals, offers a multi dimensional approach for deciphering organic matter sources
- Elevated Chlorophyll-*a* and sterol concentrations and contemporaneous increase in the particle reactive micronutrients during the spring sampling period capture seasonal influx of relatively fresh phytodetritus.
- Connectivity to adjacent watershed facilitates offshore transport of "aged" terrestrial organic matter and nutrients

6

Seasonal variability in the source and composition of particulate matter in the depositional zone of Baltimore Canyon, U.S. Mid-Atlantic Bight

9   Prouty[1]*, N.G., Mienis[2], F., Campbell[1], P., Roark[4], E.B., Davies[5], A.J., Robertson[5], C.M., Duineveld[2],
10 G., Ross[6], S.W., Rhode[7], M., Demopoulos[8], A.W.J.

11 [1] US Geological Survey, Pacific Coastal and Marine Science Center, 2885 Mission Street, Santa Cruz,
12 CA 95060 nprouty@usgs.gov
13 [2] NIOZ Royal Netherlands Institute for Sea Research and Utrecht University, P.O. Box 59, 1790 AB
14 Den Burg The Netherlands
15 [4] Department of Geography, Texas A&M University, College Station, TX 77843
16 [5] School of Ocean Sciences, Bangor University, Menai Bridge Anglesey, LL59 5AB, UK
17 [6] University of North Carolina-Wilmington, Center for Marine Science, 5600 Marvin Moss Ln,
18   Wilmington, NC 28409
19 [7] 518 McEnery Ally, Charleston, SC 29412
20 [8] US Geological Survey, Wetland and Aquatic Research Center, 7920 NW 71st St., Gainesville, FL
21   32653
22 *corresponding author*

23

24 **Abstract**

25 Submarine canyons are often hotspots of biomass due to enhanced productivity and funneling of

26 organic matter of marine and terrestrial origin. However, most deep-sea canyons remain poorly studied

27 in terms of their role as conduits of terrestrial and marine particles. A multi-tracer geochemical

28 investigation of particles collected yearlong by a sediment trap in Baltimore Canyon on the US Mid-

29 Atlantic Bight (MAB) revealed temporal variability in source, transport, and fate of particulate matter.

30 Both organic biomarker composition (sterol and *n*-alkanes) and bulk characteristics ($\delta^{13}C$, $\Delta^{14}C$, Chl-*a*)

31 suggest that while on average the annual contribution of terrestrial and marine organic matter sources

32 are similar, 42% and 52% respectively, marine sources dominate. Elevated Chlorophyll-*a* and sterol

33 concentrations during the spring sampling period highlight a seasonal influx of relatively fresh

34 phytodetritus. In addition, the contemporaneous increase in the particle reactive micronutrients

35 cadmium (Cd) and molybdenum (Mo) in the spring suggest increased scavenging, aggregation, and

36 sinking of phytodetrital biomass in response to enhanced surface production within the nutricline.

37 While tidally driven currents within the canyon resuspend sediment between 200 and 600 m, resulting

38 in the formation of a nepheloid layer rich in lithogenic material, near-bed sediment remobilization in

39 the canyon depositional zone was minimal. Instead, vertical transport and lateral transport across the

40 continental margin were the dominant processes driving seasonal input of particulate matter. In turn,

41 seasonal variability in deposited particulate organic matter is likely linked to benthic faunal

42 composition and ecosystem scale carbon cycling.

43

44 **Keywords**
45 Submarine canyons; deep-sea ecosystems; sediment trap; geochemical analyses; organic matter
46
47

48 **1. Introduction**

49 Submarine canyons play a key role in modulating the flux of particulate organic and inorganic matter

50 to the deep ocean, particularly given that continental shelves and slopes are productive and dynamic

51 ocean margin systems. As a result, canyons are often conduits for the transport of sediments, organic

52 matter, and contaminants from continental margins to the abyssal plain, providing effective

53 connections between highly productive shelf waters and the food limited deep-sea (Canals *et al.*, 2006;

54 Palanques *et al.*, 2006; Costa *et al.*, 2011; Levin and Sibuet, 2012; Puig *et al.*, 2012). Contemporary

55 sedimentary processes within canyons include storm induced turbidity currents, advection through

56 shelf resuspension, slope failures, internal waves, trawling, and dense shelf cascading (see review by

57 Puig *et al.*, 2014). Through the channeling and concentrating of organic matter via dynamic physical

58 processes, canyon fauna can experience enhanced food supply (Vetter and Dayton, 1998; Duineveld *et*

59 *al.*, 2001; De Leo *et al.*, 2010). Therefore, submarine canyons can potentially be hotspots of

60 biodiversity where enhanced fluxes of organic matter and deposition sustain tremendous benthic

61 biomass in the deep sea compared with nearby open slope habitats at similar depths (Levin *et al.*, 2001;

62 Garcia *et al.*, 2007; De Leo *et al.*, 2010). Within canyons, different physical regimes can substantially

63 alter the organic composition of sediments and the abundance of fauna thriving on these resources. For

64 example, local deposition centers of sediment and organics are hotspots of detritivorous bottom

65 dwelling organisms in the Portuguese Nazaré and New Zealand's Kaikoura canyons (De Leo *et al.*,

66 2010). Furthermore, episodic events known to affect benthic biomass and biodiversity, such as

67 sediment cascades enriched in organic matter (Canals *et al.*, 2006), or increased seasonal productivity

68 in surface waters due to upwelling along canyon edges (Soltwedel, 2000; Garcia *et al.*, 2007; Howatt

69 and Allen, 2013), can temporarily trigger increased sedimentation and/or food availability.

70

71 Submarine canyons are a major feature incising the United States Atlantic continental margin, from

72 Cape Hatteras to Atlantic Canada. In this region, canyons act as conduits and reservoirs of shelf-

73 sourced sediments, transporting this material from the shelf to the slope. The MAB shelf within or near

2

74   canyons is known for high organic inputs resulting from enhanced surface water productivity (Schaff

75   *et al.*, 1992; DeMaster *et al.*, 1994; Rex and Etter, 2010). This region also contains a high diversity of

76   unique habitats within a relatively small area, some recognized as rich coral habitats and important

77   areas for the diversity of the MAB (Hecker, 1980; Hecker *et al.*, 1983). The MAB is incised by 13

78   major canyons of varying size, shape, and morphological complexity (Obelcz *et al.*, 2014). Baltimore

79   Canyon represents one of the best studied canyons in this region (e.g., Gardner, 1989a, b) and was the

80   focus of a multi-year study to better understand the unique hard bottom and soft-sediment communities

81   within and adjacent to the canyon (Brooke and Ross, 2014; Brooke *et al.*, 2016). Recent results from

82   Baltimore Canyon have identified discrete resuspension and deposition zones in the upper canyon and

83   the deeper part of the canyon, respectively. Differences in benthic infaunal communities of Baltimore

84   Canyon appear to be linked to this zonation, as previously documented in other canyon and margin

85   settings where benthic community patterns vary with depth and organic matter (OM) content (e.g.,

86   (Carney *et al.*, 2005; Gibson *et al.*, 2005; Wei *et al.*, 2010). For example, in Baltimore Canyon reduced

87   infaunal diversity and enhanced infaunal density observed at 900 m was coincident with a zone of

88   organically enriched, finer sediments, characterizing the depositional zone (840 to 1180 m) of the

89   lower reaches of the canyon. In addition to spatial patterns of sediment deposition and organic

90   composition, temporal variations in the transport of both marine and terrestrial organic matter can

91   impact benthic community composition and trophic status (Pusceddu *et al.*, 2009), as well as the deep-

92   sea carbon cycle through changes in ingestion, assimilation, and respiration (e.g., Vetter and Dayton,

93   1998; Hunter *et al.*, 2013). For example, Hunter et al. (2013) observed changes in macrofaunal feeding

94   activity and bacterial C uptake as a result of changes in particulate organic matter (POM) composition.

95   Therefore seasonal variations in organic matter flux are key factors influencing deep-sea ecosystems

96   (Gooday, 2002).

97

98   A major aim of this study is to better understand the provenance signature of particle (food) delivery

99   within a submarine canyon by analyzing a suite of geochemical tracers (e.g., stable and radio-isotopes,

100   lipid biomarkers, ^{210}Pb, trace metals) collected during a 1-year sediment trap deployment and CTD

101   profiling. While an arsenal of biomarker compounds (e.g., *n*-alkanes, sterols, fatty alcohols, fatty acids,

102   lignin phenols) exist to identify biotic sources as well as yield information on decomposition and

103   diagenesis (e.g., Bianchi and Canuel, 2011 and references therein), ambiguities do exist when

104   elucidating sources of organic matter based on biomarker composition given overlapping sources (e.g.,

105   Volkman *et al.,* 2008). Therefore, combining the *n*-alkane and sterol biomarker results with the other

106   tracers (i.e., stable isotopes, trace metals, radiocarbon) presented here offers a multi dimensional

107   approach for deciphering organic matter sources (e.g., Wakeham and McNichol, 2014). By building

108   on previous research demonstrating the utility of hydrocarbons as tracers of organic matter source in

109   the aquatic ecosystem (e.g., Volkman, 1986; Meyers, 1994; Goni *et al.*, 1997; Wakeham *et al.*, 1997;

110   Eglinton and Eglinton, 2008; Wakeham and McNichol, 2014), we can investigate the primary sources

111   of organic matter within Baltimore Canyon. Taken together this detailed study highlights for the first

112   time key observations describing the temporal variability of organic matter flux that influences the

113   deep-sea ecosystems within Baltimore Canyon

114

115   **2. Materials and Methods**

116   *2.1 Study Area: Baltimore Canyon*

117   Baltimore Canyon, a shelf-sourced canyon is located approximately 125 km southeast of the entrance

118   to Delaware Bay, extends for a distance of 25 km until it merges onto the abyssal plain at a depth of

119   1500 m (Fig. 1). Near the head of the canyon, the width is 3 km and increases to 8 km at the shelf

120   break at a depth of 100 m. Several meanders characterize the canyon, with the canyon axis curving

121   southward at the upper reaches and then turning eastward with increasing depth until it is oriented east-

122   west at 3000 m water depth (Obelcz *et al.*, 2014) (Fig. 1). A series of bathymetric steps and terraces

123   are found near the head of the canyon where the cross-sectional profile is V-shaped and transitions into

124   a U-shaped canyon at 1000 m (Obelcz *et al.*, 2014).

125

126   Sediment supply to Baltimore Canyon is from the pelagic zone and reworked shelf sediment (Gardner,

127   1989b) mainly transported via off-shelf spill in canyon heads, failure of the steep canyon walls, and

128   resuspension by bottom currents and internal waves (Obelcz *et al.*, 2014), as well as small-scale mass

129   wasting events triggered by bioerosion (Valentine *et al.*, 1980). Within the canyon, currents focused by

130   the canyon axis in the form of tidal bores and internal waves resuspend sediment between

131   200 and 600 m and sometimes down to 800 m allowing these sediments to be transported down canyon

132   along density surfaces (Gardner, 1989a, b). Resuspension occurs primarily during flood and to a lesser

133   extent during ebb flows and is most intense and episodic when the water is poorly stratified

134   (i.e., during late winter and early spring), though episodic events may occur at other times of the year

135   (Gardner, 1989a, b).

136

137   *2.2 Sediment Traps*

138   Two benthic landers, each consisting of an aluminum tripod frame approximately 2 m in height

139   equipped with twin acoustic releases and eight buoyancy spheres were deployed on September 5, 2012

140   at a depth of 603 m (38° 09.024 N, 73° 50.954 W, described as the shallow lander) and at 1318 m (38°

141   02.543 N, 73° 44.153 W, described as the deep lander) (Fig. 1). Each lander was equipped with a

142   Technicap PPS 4/3 sediment trap programmed to rotate a 250 mL sample bottle at either 20 or 30-day

143   intervals, delivering 12 samples during the 1-year deployment. Temperature, salinity, turbidity,

144   dissolved oxygen, and bottom currents were measured using an Aanderaa (RCM) string logger. All

145   RCM probes were mounted approximately 1.5 m off bottom with the exception of the current meter,

146   which was approximately 2 m off the bottom. In addition, a mooring was deployed August 18, 2012 at

147   1082 m (38° 04.657 N, 73° 46.957 W, described as the mid-mooring) (Fig. 1). The mooring was

148   equipped with a Honjo Parflux sediment trap with thirteen 500 mL bottles mounted 4 m above bottom

149   programmed to rotate on a 30-day interval. The sampling design enabled the examination of canyon

150   characteristics, including the movement of particulate material up and down canyon, propagation of

151   internal waves, water parameter variability, and particle fluxes.

152

153   Biological activity in the sediment traps was inhibited by treating the traps with a pH buffered solution

154   of mercuric chloride ($HgCl_2$) in seawater, which has been shown to be an effective means to limit

155   microbial activity and subsequent alteration of organic matter (e.g., Lee *et al.*, 1992). While not

156   immune to diagenesis/degradation within the water column (e.g., Wakeham *et al.*, 1997; Tolosa *et al.*,

157   2003), the retention of a "biological heritage" of lipid extraction (e.g., *n*-alkanes and sterols) from

158   sediments is less sensitive to alteration and degradation and represents important organic geochemical

159   proxies that are preferentially preserved relative to other classes of biomarkers (see reviews by

160   Volkman, 1986; Meyers, 1994; Eglinton and Eglinton, 2008). Early on Prahl *et al.* (1980)

161   demonstrated a decrease in aliphatic hydrocarbon distribution in surface sediments relative to trap

162   sediment. Similarly, previous work has demonstrated the preferential removal of labile components

163   and enrichment of residual recalcitrant matter in surface sediment relative to trap material (e.g.,

164   Wakeham and Canuel, 2006; Wakeham and McNichol, 2014).

165

166   The complete time-series from the shallow (603 m) and mid-depth (1082 m) trap sites were

167   compromised by mass flux events (in October 2012) that filled the trap funnels completely, leaving

168   only a few samples intact. The flux estimate may be unreliable since the elevated current speeds

169   surpass the settling velocity of particles (Knauer and Asper, 1989). The only sediment trap with an

170   almost complete sampling series was retrieved from the deepest Baltimore Canyon lander site (1318

171   m). The missing dates represent sediment trap bottles that were partially open upon retrieval, therefore

172   precluding accurate flux measurements and sample preservation.   Sediment trap samples were split

173   into five equal splits with a rotor splitter at the Royal Netherlands Institute for Sea Research (NIOZ).

174   Two splits were rinsed thoroughly to remove sea salt and $HgCl_2$, after which they were frozen, freeze

175   dried, and weighed to calculate mass fluxes and prepared for geochemical analyses. To keep samples

176   intact for pigment analysis, another split was rinsed with filtered seawater from the deployment site

177   after which it was freeze dried.

178

179   *2.3   Water column properties*

180   Vertical profiles were made of the water column properties using a CTD-rosette (SBE 911*plus* CTD

181   profiler and a rosette containing twelve 5 L Niskin bottles) deployed inside Baltimore Canyon to

182   establish if the canyon acts as conduit for suspended and dissolved material. One CTD transect was

183   taken down the axis of the canyon, and during these casts, the CTD array was lowered from the surface

184   to as close to the bottom as feasible (usually about 10 m above bottom) (Fig. 1). Seawater samples

185   were collected during the upcast of the CTD at shallow (250 m), mid (644 m), and deep (1140 m) sites

186   within Baltimore Canyon, as well as at mid-depth shelf sites (678 m) outside the canyon for

187   measurements of nutrient concentrations, trace metals, and POM (>0.45 μm). Seawater was filtered

188   directly from the Niskin bottles using acid-cleaned Teflon coated tubing attached to a polypropylene

189   filter holder that was preloaded with an acid-cleaned polysulfone filter and attached to a vacuum pump.

190   Filters were pre-cleaned by soaking in trace metal grade HCl in a 1 L low-density polyethylene bottle.

191   Replicate water samples were collected from two 5 L Niskin bottles at each sampling depth. Water

192   column particulate matter for trace element measurements was collected by filtering approximately 5 L

193   of seawater on acid-cleaned 0.45 μm polysulfone filters (47 mm) given low blank concentrations

194   (Planquette and Sherrell, 2012). The filter holders with preloaded filters were double bagged in

195   polyethylene zip-lock bags and kept frozen for transport back to the laboratory.

196

197   Seawater samples collected for dissolved nutrient analysis were stored in acid-cleaned high-density

198   polyethylene 20 mL scintillation vials, which were triple washed with extra filtrate before saving the

199   final sample for analysis. These samples were frozen immediately until analyzed at the Geochemical

200   and Environmental Research Group at Texas A&M University, College Station. Nutrient samples were

201   analyzed on an Astoria-Pacific auto-analyzer. The nitrate/nitrite/silicate methods are based on

202   Armstrong *et al.* (1967). Phosphate methods are based on Bernhardt and Wilhelms (1967). Ammonium

203   methods are based on Harwood and Kühn, (1970). The dissolved inorganic nitrogen (DIN)

204   concentrations were calculated as the sum of nitrite, nitrate, and ammonium concentrations. Analytical

205 detection limits were 0.01 µM for phosphate, 0.003 µM for nitrite, 0.05 µM for nitrate and silicate, and

206 0.08 µM for ammonium.

207

208 *2.4 Geochemical Analyses*

209 Sediment organic carbon and nitrogen content were measured on a Thermo Organic Elemental

210 Analyser Flash 2000, and stable carbon and nitrogen isotopes were measured on a Thermo Delta V

211 Advantage Isotope Ratio MS at NIOZ. Prior to analysis, samples for C_{org} and $\delta^{13}C$ analysis were

212 acidified with HCl to remove all inorganic carbon. Standards used for C were acetanilide and benzoic

213 acid, respectively (analytical detection limits $\delta^{13}C = 0.3‰$). Samples for %N and $\delta^{15}N$ analysis were

214 not acidified and standards used were acetanilide and urea respectively (analytical detection limits $\delta^{15}N$

215 $= 0.1‰$). Trace element concentrations of the suspended particulate matter and sediment trap material

216 were determined by ICP-MS at the USGS Mass Spectrometry Facilities in Denver, Colorado. Filters

217 were digested following procedures outlined in Planquette and Sherrell (2012). Data presented here

218 were reported in µg g^{-1} following blank correction, as determined from digesting procedural filter

219 blanks, and sample and filter weight corrections (Prouty *et al.*, 2016). For the sediment traps, 50 to

220 100 mg of sediment was digested using a 4-acid procedure ($HF + HCl + HNO_3 + HClO_4$), taken to

221 dryness, and the residue dissolved in 5 to 20 mL of 5% to 13% HNO_3 with a dilution factor of 10^3 to

222 10^4 (Briggs and Meier, 2002).

223

224 Concentrations of chlorophyll *a* and its derivatives (phaeophorbides, phaeophytines) were determined

225 with reverse-phase HPLC according to the method outlined by Witbaard *et al.*, (2000). Phytopigments

226 were identified and quantified using a library based on pigment standards (DHI, Denmark). From the

227 results of the pigment analysis, intact chlorophyll-*a* concentrations were taken as a proxy for fresh

228 phytodetritus biomass. The chlorophyll-*a*/phaeopigment ratio was used to indicate the freshness of the

229 trapped phytodetritus. The activity of ^{210}Pb was determined by alpha spectrometry from ^{210}Po using a

230 Canberra alpha detector, which was extracted from the sample by leaching with concentrated HCl

231 (Boer et al., 2006). The ^{210}Pb activity of sediment trap samples was used as an indicator for the relative

232 proportion of suspended and freshly settled material. Fresh settled material has a high ^{210}Pb signal,

233 while resuspended material shows lower values due to radioactive decay.

234

235 Sediment radiocarbon (^{14}C) ages were determined at the National Ocean Sciences Accelerator Mass

236 Spectrometry (NOSAMS) facility, Woods Hole, MA USA. Approximately 50 mg of acidified (1.2N

237 HCl) bulk sediment was converted to CO_2 and graphitized for accelerator mass spectrometry (AMS)

238   (Vogel *et al.*, 1987). Radiocarbon ages were calculated using the Libby half-life of 5568 years. The

239    $D^{14}C$ values (i.e., radiocarbon values without age correction) were age corrected to account for decay

240   that took place between collection (or death) and the time of measurement using the following

241   equation: $\Delta^{14}C = (Fm*\text{age correction})-1)*1000$ where age correction is defined as exp((1950-year of

242   measurement)/8267), and Fm is fraction modern (Stuiver and Polach, 1977). Radiocarbon results are

243   reported as $\Delta^{14}C$ (‰) and conventional radiocarbon age after applying a measured $\delta^{13}C$ correction

244   (Stuiver and Polach, 1977).

245

246   Molecular composition of the sediment trap samples was determined by gas chromatography-mass

247   spectrometry (GC-MS) at the USGS Pacific Coastal Marine Science Center's (PCMSC) Organic

248   Geochemistry laboratory in Santa Cruz, California as described in Prouty *et al.* (2016). Approximately

249   1-2 g of freeze-dried organic matter was extracted by pressurized solvent extraction (ASE, Dionex

250   Corp., CA, USA). Samples were extracted with a hexane:acetone (1:1) solvent mixture followed by a

251   second extraction in dichloromethane:methanol (2:1) solvent mixture. Internal standards (5-α-

252   androstane, 5-α-androstan-3-β-ol) were added to samples prior to extraction. All glassware was

253   washed, solvent rinsed (methanol, hexane, and dichloromethane), and combusted at 400°C overnight.

254   Blanks were run for the entire procedure, including extraction, solvent concentration, and purification.

255   After evaporation of extracts to 5 ml volume utilizing TurboVap Evaporation Concentrator (Zymark

256   Corp., NC,USA), samples were loaded onto liquid chromatography columns for compound class

257   separation. Each column was layered with 2.5 g of 5% deactivated alumina, 2.5 g of 62 silica gel and

258   5.0 g of 923 silica gel, which had previously been activated at 500° C for 8 h and then, in the case of

259   the alumina, partially deactivated with ultrapure water (5% w/w). Three separate fractions were

260   collected: F1-saturate (100% hexane eluent); F2-aromatic (30% DCM : 70% hexane eluent); and, F3-

261   polar (50% ethyl acetate: 50% hexane) and reduced in volume to 1.0 ml. The polar fraction (F3) was

262   further derivatized with BSTFA (N,O-bis(trimethylsilyl) trifluoroacetamide) containing 2% TMCS

263   (trimethylchlorosilane) and anhydrous acetonitrile. Extracts were analyzed by splitless injection onto

264   an Agilent 6890 gas chromatograph interfaced to an HP 5973 mass spectrometer (GC-MS) at the

265   USGS PCMSC Organic Geochemistry Laboratories in Santa Cruz, CA. The gas chromatograph oven

266   program had an initial temperature of 90°C which was held for 4.0 min then ramped at 5°C min $^{-1}$ to a

267   final temperature of 310°C which was held at this final temperature for 10 min. The capillary column

268   (DB-5MS: 30 m length, 0.25 mm id with a 25 μm phase thickness) was directly interfaced to the ion

269   source of the mass spectrometer. Hexane instrument blanks and procedural sample duplicates were

270   run and analyzed for every 10 samples. Compound identifications were made by comparison with

271 known analytical standards and/or published reference spectra (Fig. S1). Concentrations of individual

272 lipids are blank corrected values. Lipid biomarkers (sterol and *n*-alkane) concentrations (μg g^{-1}) are

273 reported normalized to organic carbon of dry sediment as measured by a coulometer at the PCMSC.

274

275 Major organic matter sources to the sterol and *n*-alkane molecular signatures were investigated by

276 calculating relative proportions of marine, terrestrial, and anthropogenic/petroleum contributions.

277 Relative contributions from natural (marine versus terrestrial) and anthropogenic organic matter *n*-

278 alkane and sterol sources were calculated following a modified designation from Pisani *et al.* (2013).

279 Terrestrial organic matter composition of sediments was quantified using concentrations of

280 odd-numbered *n*-alkanes in the C_{21} to C_{31} range as well as the sterols campesterol, stigmasterol,

281 β-sitosterol and stigmastanol (the reduced from of stigmasterol). Marine components were determined

282 using concentrations of the sterols cholesterol, 22-dehydrocholesterol, brassicasterol, and cholestanol

283 (reduced form of cholesterol) as well as odd- and even-numbered *n*-alkanes in the C_{15} to C_{19} range.

284 The anthropogenic components were determined using the sterol composition of coprostanol,

285 epicoprostanol, and the ketone, 5-β-coprostanone, in addition to the isoprenoid hydrocarbons pristane

286 and phytane.

287
288 **3. Results and Discussion**
289

290 *3.1 Environmental and Water Column Variability*

291 The three benthic observatories positioned throughout the canyon recorded decreases in current speed,

292 turbidity, and temperature with depth (Fig. 2). The shallow lander (603 m) was positioned in the most

293 dynamic area of the canyon, with temperatures fluctuating between 4.5- 8.6 °C and a mean of 5.4 °C

294 (standard deviation [SD] 0.47 °C). The intensity of the current also varied greatly, with peak current

295 velocity reaching 66.2 cm s^{-1} and a mean of 13.7 cm s^{-1} (SD 9.03 cm s^{-1}). Peaks in turbidity appeared

296 to correspond with temperature fluctuations (Spearman's Rank Correlation on 24 hour moving average

297 data for first deployment, $r = 0.48$, $p < 0.001$). In contrast, the mid-mooring area (1082 m) was cooler

298 (temperatures between 4 °C-5.1° C and a mean of 4.5 °C [SD 0.16 °C]) and had a lower current

299 velocity (maximum current velocity: 42.3 cm s^{-1}, and mean: 8.7 cm s^{-1} [SD 5.6 cm s^{-1}]). Current

300 velocity and temperature were positively correlated at the mid-mooring location (Spearman's Rank

301 Correlation on 24 hour moving average data for first deployment, $r = 0.43$, $p < 0.001$). The deeper

302 region of Baltimore Canyon (1318 m) was cooler and had lower current velocities (temperatures

303 between 3.8-4.74 °C with a mean of 4.2 °C [SD 0.16 °C]) relative to the shallower deployments.

304 Maximum current velocity was 29.2 cm s^{-1}, with a mean speed of 6.6 cm s^{-1} [SD 3.27 cm s^{-1}]. At the

305   deep site, peaks in turbidity were positively correlated with current velocity (Spearman's Rank

306   Correlation on 24 hour moving average data for first deployment, $r = 0.62$, $p < 0.001$), and there was a

307   strong positive relationship between current velocity and temperature (Spearman's Rank Correlation

308   on 24 hour moving average data for first deployment, $r = 0.75$, $p < 0.001$), consistent with the patterns

309   recorded by the shallow and mid-canyon instruments. All sites indicated that warmer, sediment-laden

310   waters are transported to the deeper parts of the canyon during part of the tidal cycle. Current driven

311   bed shear stress (>0.1 N m^{-2}) was calculated from the sediment density and grain size, as well as the

312   kinematic viscosity and density of the seawater. Based on this calculation, sediment remobilization

313   varied throughout the canyon, with current driven bed shear stress sufficient to resuspend fine-grained

314   material (i.e. <34 μm) 15% of the time at the shallow area of the canyon, but only 1% at the mid

315   canyon and less than 0.02% in the deeper area. Plots of progressive current vectors demonstrated a

316   strong tidal flow at the shallow lander station, with a general movement towards the northeast, up

317   canyon. However, some disruption to this pattern was observed during certain periods throughout the

318   year when flow moved down canyon (Fig. 1). The canyon walls steered water movement within the

319   mid-canyon station, but disruption to the general up-canyon movement was detected during September

320   to November and January to March (Fig. 1b). During the periods of October to November 2012 and

321   March to May 2013, turbidity events in the shallow lander site were followed by a 2 °C temperature

322   increase, and accentuated by elevated current speeds and flow to the north (Fig. S2), suggesting a

323   possible link to benthic storms associated with Gulf Stream meanders and rings (Gardner *et al.*, 2017).

324   This signal was less distinct in the deeper sites where temperature fluctuations were substantially

325   smaller. The deep lander had the most consistent residual flow that was identical in direction to the

326   shallow station (Fig. 1a and c). However, such transport was less tidally regulated than in the shallow

327   station demonstrating a greater movement to the northeast.

328

329   The CTD transects conducted in Baltimore Canyon reveal a large intermediate nepheloid layer

330   extending from the mouth of the canyon from 200 m to approximately 900 m (Fig. 3), with enhanced

331   turbidity during both up and down canyon flow. This nepheloid layer was also observed by Gardner,

332   (1989a, b), and likely forms a permanent feature in Baltimore Canyon in response to internal wave

333   energy at tidal frequencies. The nepheloid layer, between 400 and 800 m, and a second, smaller patch

334   in the surface water near the canyon wall (8 km down canyon) (Fig. 3), was characterized by increased

335   lithogenic material, specifically aluminum (Al), neodymium (Nd), Iron, (Fe), and lanthanum (La) (Fig.

336   4). Particulate (>0.45 μm) element concentrations were enriched at the shallow (NF-2012-138; 261 m)

337   and mid-depth (NF-2012-128; 644 m) CTD stations whereas trace element profiles at the deep (NF-

338   2012-130; 1140 m) and slope (NF-2012-149; 668 m) CTD stations did not exhibit elevated trace metal

339   particulate concentrations at 600 m (Fig. 4). Trace element composition for the Baltimore Canyon

340   slope site was consistently low and the deep site only showed a slight enrichment near the bottom (NF-

341   2012-130; 1140 m). These results indicate that the nepheloid layer appears restricted to within the

342   canyon and to a depth of 850 m.

343

344   Nutrient profiles in Baltimore Canyon displayed surface-water depletion and bottom-water enrichment

345   in nitrate, phosphate, and dissolved silicate (Fig. 5). These results illustrate the uptake of nutrients

346   within the nutricline due to biological processes, particularly the growth of phytoplankton in the photic

347   zone. The interaction between phytoplankton growth and nutrient uptake is illustrated in the inverse

348   relationship between the nutrient and dissolved oxygen (O_2) profiles (Fig. 5). Below the mixed layer,

349   concentrations of nitrate, phosphate, and dissolved silicate were conservative and exhibited a

350   homogenous distribution at depth. The nutricline in Baltimore Canyon was defined from nutrient

351   profiles collected during the August 2012 sampling cruise. Maximum nutrient concentrations occurred

352   at ~250–300 m, consistent with the thermocline depth in Baltimore Canyon, and agrees with those

353   derived from Ocean Data Viewer (latitude 73° 49.36 N, longitude 38°23.24 W; Schlitzer, 2016). Given

354   the similarity between the individual depth profiles down canyon, the nutricline appears to be

355   homogenous along the length of the canyon with little spatial variability.

356

357   *3.2 Sediment Traps*

358   The sediment trap data at the deep site illustrate a narrow range of mass fluxes during the first seven

359   months (4.7 to 9 g m^{-2} d^{-1}) and slightly lower mass flux during the last three months (Fig. 6). There

360   were two periods of relatively elevated mass flux, September−October 2012 and January−February

361   2013. The increase in mass flux in September−October 2012 at the deep trap site indicates a

362   resuspension or mass-wasting event, potentially, linked to increase mass fluxes at the shallow and mid-

363   depth sites, and subsequent overfilling of the funnels at these shallower depths. Similar sediment trap

364   overfilling was observed in Nazare Canyon, in response to storm-induced turbidity currents (Martín *et*

365   *al.*, 2011). However, we did not observe overfilling at the deep sediment trap site, suggesting that

366   sediment loading in the shallow and mid-depth regions may not necessarily be transported along the

367   canyon thalweg to the deeper region, and that localized overspill from the canyon walls can help

368   explain asynchronous mass fluxes within the canyon. At the deep trap site, percent C_{org} and total N did

369   not vary significantly between periods and patterns of C and N fluxes and therefore closely resembled

370   those of the mass flux, with a small range in C:N ratios (8.8 to 10.6) (Table 1). ^{210}Pb activity at the

371   deep trap site displayed an inverse temporal pattern relative to mass flux. Higher mass fluxes

372   corresponded to low ^{210}Pb values (R=-0.90), indicating trapping of resuspended material (Fig. 6a).

373   Chlorophyll-*a* concentrations showed more variability between successive samples. Peak Chl-*a* flux

374   occurred in May−June 2013, coincident with elevated %C_{org} values and highest Chl- *a* /phaeopigment

375   ratio, indicating a supply of relatively fresh phytodetritus from the spring phytoplankton bloom (see

376   below). A secondary peak in Chl- *a* flux and ^{210}Pb was observed in October−November 2012,

377   indicating enhanced transport of phytodetritus (Fig. 6b).

378

379   There was a narrow range in stable carbon (δ^{13}C) and nitrogen (δ^{15}N) isotope values -22.8‰ (SD 0.15)

380   and 4.83‰ (SD 0.23) (Table 1), consistent with a marine signature (Meyers, 1994). The δ^{13}C range

381   was consistent with that reported for POM in the surface and mid-water depths, and δ^{15}N values were

382   consistent with surface POM values on the Northwest Continental Shelf (Oczkowski *et al.*, 2016). The

383   trap material most likely reflects a combination of freshly exported material and suspended POM.

384   Romero-Romero *et al.* (2016) were able to use stable isotope signatures to distinguish organic matter

385   sources in the Aviles submarine canyon. However, in our study it was difficult to distinguish between a

386   mixture of marine algae plus terrestrial C3 plants given the narrow range of sediment trap bulk δ^{13}C

387   values (-22.8 to -22.0 ‰). The enriched C:N ratios relative to the Redfield ratio (6.7; Table 1) suggests

388   a mixture of sources of both marine phytodetritus and land-derived organic debris. As shown in Figure

389   7, the sediment trap samples fall along a mixing line between marine algae and C3-vascular plants

390   according to δ^{13}C and C:N values (Goñi *et al.*, 2003; Tesi *et al.*, 2007).

391

392   The total concentration of *n*-alkanes for sediment trap samples from the deep lander site represents a

393   resolved *n*-alkane range from C_{14} to C_{32} as well as detectible amounts of the isoprenoid hydrocarbons

394   pristane (pr) and phytane (ph) (Table 2a). Total *n*-alkane concentrations ranged from <1 to 12 µg g^{-1}

395   dry weight normalized to organic carbon (µg g^{-1} C), with September/October 2012 yielding elevated

396   *n*-alkane concentrations (Fig. 6b). Overall, the molecular composition was dominated (95%) by higher

397   molecular weight (HMW, >C_{21}) *n*-alkanes, particularly *n*-C_{29} and *n*-C_{27}, except in February 2013 when

398   *n*-C_{24} was anomalously elevated (Table 2a). The Carbon Preference Index (CPI) is often used to

399   identify organic matter source by describing the molecular distribution of odd number *n*-alkanes

400   relative to even number *n*-alkanes (Bray and Evans, 1961). Overall, there was a strong odd-to-even

401   predominance, with a CPI consistently >1.0, particularly in September/October and June/July (Table

402   2a), suggesting increased OM originating from land plant material (Hedges and Parker, 1976). The

403   dominance of terrestrial plant input relative to aquatic macrophytes is also expressed through the

404   Alkane Proxy (Paq) (Ficken *et al.*, 2000). The Paq values were consistently <1, revealing the

405   dominance of long chain-length *n*-alkanes. Phytane was detected in the samples from

406   September/October of 2012, but was absent from the other months. The sediment trap sample from

407   May 2013 contained enriched pristane relative to the other months, but overall both pristane and

408   phytane concentrations were <1 µg g^{-1} C (Table 2a). Total sterol concentrations ranged from 1 to 30 µg

409   g^{-1} C (Table 2b), and were dominated by cholesterol. In comparison, the smallest contribution was

410   from the anthropogenic-sourced sterols, specifically coprostanol and epicoprostanol. Sterol

411   concentrations were elevated in October 2012 when cholesterol contributed 30% of the total sterol

412   concentration. A second peak in sterol concentration occurred in May 2013 and was dominated by both

413   cholesterol and cholestanol, comprising over 60% of the total sterol composition. Both sterols have

414   marine biological sources, such as biosynthesis of plankton organisms and zooplankton (Volkman,

415   1986). The sterol enrichment in the spring is tightly coupled to the peak in Chl-*a* concentrations (Fig.

416   6b), illustrating the influx of relatively fresh phytodetritus. The influx of fresh phytodetritus is also

417   consistent with the phytoplankton blooms in the spring when net primary productivity exceeded 700 g

418   C m^{-2} d^{-1} (Fig. 6d), as calculated per Behrenfeld and Falkowski (1997) for a 20 km^2 surrounding

419   Baltimore Canyon. In comparison, lower sterol and *n*-alkane concentrations during the winter months

420   reflect a reduction in surface water primary productivity (< 300 g C m^{-2} d^{-1}) during the winter season.

421

422   The distribution of biomarkers in the sediment trap organic matter indicates that delivery to the deep

423   area of Baltimore Canyon is a composite of sources (e.g., algal/phytoplankton/zooplankton

424   productivity and land-plant productivity). Anthropogenic sources were minimal, with an annual

425   average contribution of 6%, and the greatest contribution occurring in September 2012. Although high

426   pristane concentrations in sediment can be derived from zooplankton, the pristane/phytane ratios

427   observed in this study are used as indicators of a petrogenic, anthropogenic source (Blumer *et al.*,

428   1963). While on average the contributions from marine (43%) and terrestrial (52%) organic matter

429   sources were similar, seasonal variability in source contribution was observed in the biomarker time

430   series (Table 3). For example, September 2012 and May 2013 were dominated by terrestrial (76%) and

431   marine (71%) sources, respectively. Dominance by terrestrial sources in September 2012 was

432   potentially associated with a resuspension event as captured in the increased mass flux and reduced

433   ^{210}Pb values, and potentially linked to enhanced turbidity from overspill of the canyon walls. In

434   contrast, the peak in marine sources in May 2013 is attributed to increased primary production during

435   the spring bloom (Fig. 6d), when freshwater transport is at a maximum during spring discharge (Choi

436   and Wilkin, 2007), and facilitates offshore transport of both nutrients and terrestrially derived organic

437   matter.

438

439   A suite of trace elements was measured from the sediment trap samples collected at the deep lander

440   site (Table 4). Iron (Fe) and aluminum (Al) dominated the trace element composition of the sediment

441   traps, but showed little variability throughout the deployment period with average monthly Fe and Al

442   concentrations of 56 and 32 mg g^{-1}, respectively. After Fe and Al, barium (Ba), phosphorous (P),

443   strontium (Sr), and manganese (Mn) contributed to the elemental composition. Variability, evaluated

444   as percent contribution of standard deviation to total elemental concentration, was greatest for

445   cadmium (Cd) and molybdenum (Mo) at 4% and 3%, respectively. Peak values for the particle reactive

446   micronutrients Cd and Mo, occurred in April and May, with a smaller enrichment in October (Fig. 6c).

447   The spring and fall periods are also characterized by enrichment in total sterol concentration as

448   discussed above. During the deployment period, net primary production for the months of April

449   through June 2013 was 721, 698, and 775 g C m^{-2} d^{-1} respectively, whereas net primary production in

450   the fall months of Sept. through Nov. 2012 was 372, 429, and 422 g C m^{-2} d^{-1} respectively (Fig. 6d).

451   Hence, the spring phytoplankton bloom could have fueled the increase and export of fresh organic

452   matter (e.g., phytodetritus) in the canyon during this season. The elevated pigment fluxes correspond to

453   increased biomarker concentrations (especially sterols), indicating greater primary production and

454   export of marine-derived organic matter. The simultaneous increase in the phytoplankton essential

455   micronutrients of Cd and Mo during this period suggests increased scavenging, aggregation, and

456   sinking of biomass during seasonal blooms in response to enhanced surface production within the

457   nutricline (Wangersky *et al.*, 1989; Pohl *et al.*, 2004). The synchronous timing of the surface water

458   primary productivity signal relative to the sediment trap geochemistry time series suggests rapid export

459   and sinking of fresh particulate organic matter to the depositional zone of Baltimore Canyon. This

460   corresponds to a spring maximum at the shelf break/slope waters (Ryan *et al.*, 1999; Xu *et al.*, 2011),

461   and an increase in biomass on the MAB shelf during the spring and summer relative to the late fall

462   (Mouw and Yoder, 2005).

463

464   Radiocarbon ages of sediment trap material recovered from the Baltimore Canyon deep lander site

465   ranged between 980 (SD 15) and 1280 (SD 20) ^{14}C YBP with an average age of 1096 ^{14}C YBP

466   (SD 18) (Table 5). The most negative Δ^{14}C value (-153.75‰) occurred in the first month of the

467   deployment (September 2012), with little variability in Δ^{14}C ($\Delta\Delta^{14}$C of 30‰) observed throughout the

468   remaining part of the year. In comparison, fresh organic matter, as defined by coral tissue Δ^{14}C values,

469   was 30‰, consistent with surface water dissolved organic carbon $\Delta^{14}C$ values, ranging from 21 to

470   47‰. Therefore, the relatively "aged" material present in the trap suggests a mixture of marine and

471   terrestrial sources, as well as potential input from laterally advected refractory material (e.g., Druffel *et*

472   *al.*, 1986; Gordon and Goñi, 2003; Hwang and Druffel, 2003). The aged radiocarbon dates reflect

473   organic carbon that was photosynthetically fixed thousands of years ago, such as riverine carbon

474   exported from the Hudson River Watershed that has a $\Delta^{14}C$ signature of -350‰ (Raymond and Bauer,

475   2001). Fingerprinting and mixing approaches have been used in submarine canyons of the

476   Mediterranean Sea to identify relative source contributions (Tesi *et al.*, 2010; Pasqual *et al.*, 2013). In

477   our study, results of a two end-member $\Delta^{14}C$ mixing model yielded an annual average contribution

478   from terrestrial-derived carbon of ~48%, with the remaining ~52% attributed to autochthonous organic

479   matter produced from marine primary production. While selective degradation/preservation can alter

480   the source ^{14}C signature (Hwang *et al.*, 2010), results from the isotope mixing model are consistent

481   with annually averaged estimates based on molecular composition (Table 3).

482

483   Distal sources of terrestrial organic matter can be delivered via aeolian transport (Conte and Weber,

484   2002). However, surface sediment neodymium (Nd) isotope values from Baltimore Canyon and the

485   adjacent slope indicate that terrestrial sediment is primarily sourced from nearby riverine systems, such

486   as the Hudson River, where surface water moves southward, advecting riverine discharge towards

487   Baltimore Canyon and facilitating connectivity with adjacent watersheds (Ingham, 1992). Surface

488   sediments (0-0.5 cm) in the canyon were also enriched in terrestrial-derived sources of organic matter

489   relative to surface sediments on the slope (Supplementary Tables), demonstrating the accumulation of

490   terrestrial organic matter in the canyons relative to the slope. Transport of organic matter from

491   terrestrial sources is further facilitated by the presence of low-salinity, buoyant plume shelf waters on

492   the MAB (Churchill and Berger, 1998). This connectivity helps explain the terrestrial-derived organic

493   matter signature in the sediment trap samples and supports the hypothesis that submarine canyons

494   serve both as a conduit and reservoir of terrestrial organic matter to the deep sea (e.g., Tesi *et al.*,

495   2010).

496

497   *3.3 Canyon Zonation*

498   Substantial sedimentation/turbidity events prevented the collection of a complete time series for the

499   shallow and mid-depth sediment traps, precluding a comparison amongst the three deployments.

500   However, relative changes were detected for the period of overlap during the first two months

501   (September – October) that each trap was deployed. At the shallow site, mass fluxes were the greatest

502 and ^{210}Pb values were the lowest among the three trap sites (Table 1b), highlighting that resuspension

503 dominates the shallow region. This is consistent with prior work demonstrating a zone of net

504 convergence where internal tides travel up and down canyon, creating a region of elevated turbidity

505 (Gardner, 1989a, b). Within this depth zone (~ 600 m), surface sediment samples consisted of coarse

506 sand, small pebbles, and shell fragments at the sediment surface, presumably the result of local

507 winnowing of the surface layer removing the fines. Bulk geochemical characteristics from the shallow

508 and mid-depth traps were within the range observed at the deep site, indicating a mixture of marine and

509 terrestrial derived matter throughout the canyon. This is represented by the trap material data from the

510 shallow and mid-depth sites that plot along a mixing line, as reported above. Higher N:C ratios from

511 the shallow-depth mooring site could suggest both greater proportion of marine-derived organic matter

512 compared to the other sites and the dominance of fine-grained material in the deposition zones (Fig.

513 7b).

514

515 The relative molecular composition of the *n*-alkanes and sterols from the mid and shallow sites were

516 similar to those reported for the deep site (Table 3). For example, *n*-C$_{27}$ dominated the *n*-alkanes

517 composition in the shallow and mid-depth trap sites, and cholesterol was the dominant sterol.

518 However, the comparison between the three sediment traps also illustrates the accumulation and

519 channeling of terrestrial organic matter farther down canyon with total *n*-alkane concentrations an

520 order of magnitude greater at the deep site relative to the shallow and mid-depth sites, particularly the

521 HMW *n*-alkanes (Table 2a). The hydrocarbons pristane and phytane were either below detection or at

522 minimal concentrations at the shallow and mid-depth sites. Total sterol concentrations during the first

523 two months were elevated at the shallow and mid-depth sites relative to the deep site, reflecting higher

524 marine-sourced sterols exported from the nutricline (e.g., cholesterol and cholestanol). While limited in

525 scope, the down canyon comparison captures spatial variability consistent with previously reported

526 canyon depth zonation patterns.   In addition, relative to surface samples (0-0.5 cm) from the canyon,

527 surface samples from the adjacent slope yield lower terrestrial contribution, and an anthropogenic

528 component was absent from the slope surface sediment samples (Supplementary Table S4), supporting

529 the notion that canyons may serve as a conduit of terrestrial organic matter and contaminants. These

530 observations reflect the interplay of hydrodynamics and geomorphology, which channel and

531 concentrate sediment and organic matter within the canyon, leading to differences in organic matter

532 composition in Baltimore Canyon.

533

534   **4. Summary**

535 By examining a unique set of geochemical variables, this study demonstrated the relationship between

536 particulate matter composition in the context of seasonal variation in surface water biological

537 production and export through the nutricline in Baltimore Canyon. The sediment trap biomarker

538 compositions, together with bulk characteristics, indicate that both terrestrial OM and marine derived

539 OM are important food sources, suggesting that both vertical and lateral transport across the

540 continental margin are important processes to the deposition zone of Baltimore Canyon. However,

541 details in the temporal variability of the OM provenance reveal a larger contribution from marine-

542 derived OM in the spring, which is characterized by increased scavenging, aggregation, and sinking of

543 fresh, recently exported OM from the upper water column during a spring bloom. Connectivity to

544 adjacent watershed also facilitates offshore transport of "aged" terrestrial organic matter and nutrients.

545 Results presented here demonstrate how OM content and OM provenance signature can be linked to

546 seasonal events (e.g., surface productivity blooms), episodic events (e.g., resuspension), as well as

547 those processes occurring permanent, such as the presence of the nepheloid layer. Therefore,

548 variability is a key feature influencing the deep-sea food web, with faunal composition and carbon

549 cycling influenced by seasonal or episodic fluxes in particulate matter composition. Such deposition

550 patterns in turn may be the greatest contributors to canyons exhibiting biodiversity and productivity

551 maxima. With the majority of deep-sea canyons being poorly sampled, results presented here suggest

552 that the submarine canyons of the MAB region are a key contributor to global estimates of benthic

553 biomass and productivity in the deep sea by serving as conduits for transport of terrestrial and marine

554 derived organic matter.

555

567
568
569 **Figures**
570 **Figure 1**

571 Multibeam bathymetry of Baltimore Canyon showing position of benthic landers (white plus sign) and

572 mooring (white star) at the shallow (a), mid (b) and deep (c) sites. Progressive vector plots show the

573   cumulative movement of water at shallow (a), mid (b) and deep (c) sites, split into 60 day subsets

574   (black lines indicating Sept-Nov, green Nov-Jan, grey Jan-Mar, red Mar-May). Grey line and circles (i)

575   show the individual CTD casts that make up the transect along the axis of the canyon (two stations

576   were used for water sampling, ii=NF-2012-036 and iii=NF-2012-040) as shown in Figure 3. Black

577   triangles represent CTD casts used for water and trace element sampling (iv=NF-2012-138, v=NF-

578   2012-128, vi=NF-2012-051, vii=NF-2012-130, viii=NF-2012-149, ix=NF-2012-073). Note some

579   stations are shown with an offset line for clarity. Inset figure shows the location of Baltimore Canyon

580   (black box) with respect to the Mid-Atlantic Bight and neighboring states of Maryland (MD), Virginia

581   (VA) and Delaware (DE). Contour lines show depth in meters.

582

583   **Figure 2**

584   Oceanographic variables (y-axis) recorded by the shallow lander (603 m), mid-mooring (1082 m, note

585   no turbidity sensor) and deep lander (1318 m) in Baltimore Canyon. Black or white lines represent a

586   24-hour moving average. For the shallow and deep landers all sensors recorded at 1.5 m above bottom

587   except for currents at 2 m above bottom, which were recorded at a 15 min interval. For the mid-

588   mooring, current data was obtained at 14 m above bottom and temperature at 9 m above bottom.

589   Currents were recorded at a 15-minute interval. Temperature was recorded at a 5-minute interval and

590   was resampled to a 15-minute interval to match other sensors.

591

592   **Figure 3**

593   Baltimore Canyon nepheloid layer distribution along the canyon axis, derived from CTD profiles with

594   overlaid isopycnals (kg m^{-3}). Vertical lines show the position of CTD casts along the transect,

595   including extreme margins in the plot (number of casts = 9). Turbidity expressed as relative Formazin

596   turbidity units (FTU).

597

598   **Figure 4**

599   Trace element concentrations (µg g^{-1}; neodymium [Nd], lanthanium [La], aluminum [Al], and iron

600   [Fe]) in suspended particulate matter filtered (>0.45 µm) at discrete water column depths from CTD

601   casts in Baltimore Canyon and adjacent slope. Gray bar indicates zones of elevated turbidity derived

602   from CTD casts.

603

604   **Figure 5**

605 Nutrient vertical depth profiles from Baltimore Canyon sampled in 2012 along a down-canyon transect

606 for (a) nitrate, (b) phosphate, and (c) silicate (μmol L^{-1}) at four CTD stations, including NF12-036,

607 NF12-040, N12-051, and NF12-073. Dissolved oxygen (black line) derived from the CTD sensor is

608 shown for the Baltimore Canyon deep station (NF-12-040). Gray bar indicates depth of nutricline

609 defined from nutrient profiles collected during the August 2012 sampling cruise. (d) Down canyon

610 temperature (°C) profile derived from CTD casts.

611

612 **Figure 6**

613 Time-series for bulk sediment measurements and molecular biomarker composition derived from

614 ~monthly sediment trap samples deployed from September 5, 2012 to June 23, 2013. Results are

615 shown for (a) mass flux (g m^{-2} d^{-1}) and ^{210}Pb (mBq g^{-1}), (b) total sterol and *n*-alkane concentration (μg

616 g^{-1} C) and chlorophyll-*a* (mg g^{-1}), (c) cadmium (Cd) and molybdenum (Mo) (μg g^{-1}), and (d) net

617 primary production (g C m^{-2} d^{-1}; http://www.science.oregonstate.edu/ocean.productivity/index.php).

618

619 **Figure 7**

620 (a) Stable isotope composition of carbon (δ^{13}C; ‰) versus total nitrogen:organic carbon (N:C) ratio

621 from the deep sediment trap (1318 m) samples. The potential sources of organic carbon (C3 vascular

622 plants, C3 soil organic matter, heterotrophic bacteria, and marine phytoplankton) are shown to

623 highlight mixed sources of organic matter to the deep-sea sediment samples. The N:C ratio is plotted

624 versus δ^{13}C rather than the C:N ratio because the N:C ratio behaves linearly in a mixing model (Goñi

625 *et al.*, 2003). (b) Results from the shallow (603 m) and mid-depth (1082) sites relative to the deep site

626 for the months of overlap (Aug-Sept. 2012).

627

628 **References:**

629 Armstrong, F.A.J., Stearns, C.R., Strickland, J.D.H., 1967. The measurement of upwelling and
630   subsequent biological process by means of the Technicon Autoanalyzer® and associated
631   equipment. Elsevier, pp. 381-389.
632 Behrenfeld, M.J., Falkowski, P.G., 1997. Photosynthetic rates derived from satellite-based chlorophyll
633   concentration. Limnology and Oceanography 42 (1), 1-20.
634 Bernhardt, H., Wilhelms, A., 1967. The continuous determination of low level iron, soluble phosphate
635   and total phosphate with the AutoAnalyzer. pp. 385-389.
636 Bianchi, T.S., Canuel, E.A., 2011. Chemical biomarkers in aquatic ecosystems. Princeton University
637   Press. 329 pp.
638 Blumer, M., Mullin, M.M., Thomas, D.W., 1963. Pristane in zooplankton. Science 140, 974-974.
639 Bray, E.E., Evans, E.D., 1961. Distribution of n-paraffins as a clue to recognition of source beds.

640 Boer, W., van den Bergh, G.D., de Haas, H., de Stigter, H.C., Gieles, R., van Weering, T.C.E., 2006.
641   Validation of accumulation rates in Teluk Banten (Indonesia) from commonly applied ^{210}Pb
642   models, using the 1883 Krakatau tephra as time marker. Marine Geology 227 (3–4), 263-277.
643 Geochimica et Cosmochimica Acta 22 (1), 2-15.
644 Briggs, P.H., Meier, A.L., 2002. The determination of forty-two elements in geological materials by
645   inductively coupled plasma – mass spectrometry. USGS Open File Report 02-223-I.
646 Brooke, S., Ross, S.W., 2014. First observations of the cold-water coral Lophelia pertusa in mid-
647   Atlantic canyons of the USA. Deep Sea Research Part II: Topical Studies in Oceanography 104,
648   245-251.
649 Brooke, S.D., Watts, M.W., Heil, A.D., Rhode, M., Mienis, F., Duineveld, G.C.A., Davies, A.J., Ross,
650   S.W., 2016. Distributions and habitat associations of deep-water corals in Norfolk and Baltimore
651   Canyons, Mid-Atlantic Bight, USA. Deep Sea Research Part II: Topical Studies in Oceanography.
652 Canals, M., Puig, P., Durrieu de Madron, X., Heussner, S., Palanques, A., Fabres, J., 2006. Flushing
653   submarine canyons. Nature 444 (7117), 354-357.
654 Carney, R., Gibson, R., Atkinson, R., Gordon, J., 2005. Zonation of deep biota on continental margins.
655   Oceanography and Marine Biology Annual Review 43, 211-278.
656 Choi, B.-J., Wilkin, J.L., 2007. The effect of wind on the dispersal of the Hudson River Plume. Journal
657   of Physical Oceanography 37 (7), 1878-1897.
658 Churchill, J.H., Berger, T.J., 1998. Transport of middle Atlantic Bight shelf water to the Gulf Stream
659   near Cape Hatteras. Journal of Geophysical Research: Oceans 103 (C13), 30605-30621.
660 Conte, M.H., Weber, J.C., 2002. Plant biomarkers in aerosols record isotopic discrimination of
661   terrestrial photosynthesis. Nature 417 (6889), 639-641.
662 Costa, A.M., Mil-Homens, M., Lebreiro, S.M., Richter, T.O., de Stigter, H., Boer, W., Trancoso, M.A.,
663   Melo, Z., Mouro, F., Mateus, M., 2011. Origin and transport of trace metals deposited in the
664   canyons off Lisboa and adjacent slopes (Portuguese Margin) in the last century. Marine Geology
665   282 (3), 169-177.
666 De Leo, F.C., Smith, C.R., Rowden, A.A., Bowden, D.A., Clark, M.R., 2010. Submarine canyons:
667   hotspots of benthic biomass and productivity in the deep sea. Proceedings of the Royal Society of
668   London B: Biological Sciences.
669 DeMaster, D.J., Pope, R.H., Levin, L.A., Blair, N.E., 1994. Biological mixing intensity and rates of
670   organic carbon accumulation in North Carolina slope sediments. Deep Sea Research Part II:
671   Topical Studies in Oceanography 41 (4), 735-753.
672 Druffel, E.R.M., Honju, S., Griffin, S., Wong, C., 1986. Radiocarbon in particulate matter from the
673   eastern sub-arctic Pacific Ocean; evidence of a source of terrestrial carbon to the deep sea.
674   Radiocarbon 28 (2A), 397-407.
675 Duineveld, G., Lavaleye, M., Berghuis, E., De Wilde, P., 2001. Activity and composition of the
676   benthic fauna in the Whittard Canyon and the adjacent continental slope (NE Atlantic).
677   Oceanologica Acta 24 (1), 69-83.
678 Eglinton, T.I., Eglinton, G., 2008. Molecular proxies for paleoclimatology. Earth and Planetary
679   Science Letters 275 (1), 1-16.
680 Ficken, K.J., Li, B., Swain, D.L., Eglinton, G., 2000. An *n*-alkane proxy for the sedimentary input of
681   submerged/floating freshwater aquatic macrophytes. Organic Geochemistry 31 (7–8), 745-749.
682 Garcia, R., Koho, K.A., De Stigter, H.C., Epping, E., Koning, E., Thomsen, L., 2007. Distribution of
683   meiobenthos in the Nazare canyon and adjacent slope (western Iberian Margin) in relation to
684   sedimentary composition. Marine Ecology Progress Series 340, 207-220.
685 Gardner, W.D., 1989a. Baltimore Canyon as a modern conduit of sediment to the deep sea. Deep Sea
686   Research Part A. Oceanographic Research Papers 36 (3), 323-358.
687 Gardner, W.D., 1989b. Periodic resuspension in Baltimore Canyon by focusing of internal waves.
688   Journal of Geophysical Research: Oceans 94 (C12), 18185-18194.

689 Gardner, W.D., Tucholke, B.E., Richardson, M.J., Biscaye, P.E., 2017. Benthic storms, nepheloid
690   layers, and linkage with upper ocean dynamics in the western North Atlantic. Marine Geology 385,
691   304-327.
692 Gibson, R.N., Atkinson, R.J.A., Gordon, J.D.M., 2005. Zonation of deep biota on continental margins.
693   Oceanography and Marine Biology: An Annual Review 43, 211-278.
694 Goni, M.A., Ruttenberg, K.C., Eglinton, T.I., 1997. Sources and contribution of terrigenous organic
695   carbon to surface sediments in the Gulf of Mexico. Nature 389 (6648), 275-278.
696 Goñi, M.A., Teixeira, M.J., Perkey, D.W., 2003. Sources and distribution of organic matter in a river-
697   dominated estuary (Winyah Bay, SC, USA). Estuarine, Coastal and Shelf Science 57 (5), 1023-
698   1048.
699 Gooday, A.J., 2002. Biological responses to seasonally varying fluxes of organic matter to the ocean
700   floor: a review. Journal of Oceanography 58 (2), 305-332.
701 Gordon, E.S., Goñi, M.A., 2003. Sources and distribution of terrigenous organic matter delivered by
702   the Atchafalaya River to sediments in the northern Gulf of Mexico. Geochimica et Cosmochimica
703   Acta 67 (13), 2359-2375.
704 Harwood, J.E., Kühn, A.L., 1970. A colorimetric method for ammonia in natural waters. Water
705   Research 4 (12), 805-811.
706 Hecker, B., 1980. Scleractinians (stony corals) encountered in this study: Appendix C. Canyon
707   Assessment Study no. BLM-AA551-CT8-49. U.S. Department of Interior, Bureau of Land
708   Management, Washington, DC.
709 Hecker, B., Logan, D.T., Gandarillas, F.E., Gibson, P.R., 1983. Megafaunal assemblages in Lydonia
710   Canyon, Baltimore Canyon, and selected slope areas. Canyon and Slope Processes Study, Final
711   Report prepared for the U.S. Department of the Interior. Minerals Management Service,
712   Washington, D.C. .
713 Hedges, J.I., Parker, P.L., 1976. Land-derived organic matter in surface sediments from the Gulf of
714   Mexico. Geochimica et Cosmochimica Acta 40 (9), 1019-1029.
715 Howatt, T.M., Allen, S.E., 2013. Impact of the continental shelf slope on upwelling through submarine
716   canyons. Journal of Geophysical Research: Oceans 118 (10), 5814-5828.
717 Hunter, W.R., Jamieson, A., Huvenne, V.A.I., Witte, U., 2013. Sediment community responses to
718   marine vs. terrigenous organic matter in a submarine canyon. Biogeosciences 10, 67-80.
719 Hwang, J., Druffel, E.R.M., 2003. Lipid-like material as the source of the uncharacterized organic
720   carbon in the ocean? Science 299 (5608), 881-884.
721 Hwang, J., Druffel, E.R.M., Eglinton, T.I., 2010. Widespread influence of resuspended sediments on
722   oceanic particulate organic carbon: Insights from radiocarbon and aluminum contents in sinking
723   particles. Global Biogeochemical Cycles 24 (4).
724 Ingham, M.C., 1992. Summary of the physical oceanographic processes and features pertinent to
725   pollution distribution in the coastal and offshore waters of the northeastern United States, Virginia
726   to Maine. In: Ingham, M.C. (Ed.), NOAA Technical Memorandum NMFS-FNEC-17. National
727   Oceanic and Atmospheric Administration, Woods Hole, MA.
728 Knauer, G.A., Asper, V., 1989. Sediment trap technology and sampling, Report of the US JGOFS
729   working group on sediment trap technology and sampling, University of South Mississippi, USA,
730   14–16 November 1988, US JGOFS Planning report No 10, WHOI, August 1989, 94pp.
731   Lee, C., Hedges, J.I., Wakeham, S.G., Zhu, N., 1992. Effectiveness of various treatments in retarding
732   microbial activity in sediment trap material and their effects on the collection of swimmers.
733   Limnology and Oceanography 37 (1), 117-130.
734 Levin, L.A., Etter, R.J., Rex, M.A., Gooday, A.J., Smith, C.R., Pineda, J., Stuart, C.T., Hessler, R.R.,
735   Pawson, D., 2001. Environmental Influences on Regional Deep-Sea Species Diversity 1. Annual
736   Review of Ecology and Systematics 32 (1), 51-93.

737 Levin, L.A., Sibuet, M., 2012. Understanding continental margin biodiversity: a new imperative.
738   Annual Review of Marine Science 4, 79-112.
739 Martín, J., Palanques, A., Vitorino, J., Oliveira, A., De Stigter, H.C., 2011. Near-bottom particulate
740   matter dynamics in the Nazaré submarine canyon under calm and stormy conditions. Deep Sea
741   Research Part II: Topical Studies in Oceanography 58 (23), 2388-2400.
742 Meyers, P.A., 1994. Preservation of elemental and isotopic source identification of sedimentary
743   organic matter. Chemical Geology 114 (3–4), 289-302.
744 Mouw, C.B., Yoder, J.A., 2005. Primary production calculations in the Mid-Atlantic Bight, including
745   effects of phytoplankton community size structure. Limnology and Oceanography 50 (4), 1232-
746   1243.
747 Obelcz, J., Brothers, D., Chaytor, J., Brink, U.t., Ross, S.W., Brooke, S., 2014. Geomorphic
748   characterization of four shelf-sourced submarine canyons along the U.S. Mid-Atlantic continental
749   margin. Deep Sea Research Part II: Topical Studies in Oceanography 104, 106-119.
750 Oczkowski, A., Kreakie, B., McKinney, R.A., Prezioso, J., 2016. Patterns in stable isotope values of
751   nitrogen and carbon in particulate matter from the Northwest Atlantic Continental Shelf, from the
752   Gulf of Maine to Cape Hatteras. Frontiers in Marine Science 3 (252), 1-9.
753 Palanques, A., Durrieu de Madron, X., Puig, P., Fabres, J., Guillén, J., Calafat, A., Canals, M.,
754   Heussner, S., Bonnin, J., 2006. Suspended sediment fluxes and transport processes in the Gulf of
755   Lions submarine canyons. The role of storms and dense water cascading. Marine Geology 234 (1),
756   43-61.
757 Pasqual, C., Goñi, M.A., Tesi, T., Sanchez-Vidal, A., Calafat, A., Canals, M., 2013. Composition and
758   provenance of terrigenous organic matter transported along submarine canyons in the Gulf of Lion
759   (NW Mediterranean Sea). Progress in Oceanography 118, 81-94.
760 Pisani, O., Oros, D.R., Oyo-Ita, O.E., Ekpo, B.O., Jaffé, R., Simoneit, B.R.T., 2013. Biomarkers in
761   surface sediments from the Cross River and estuary system, SE Nigeria: Assessment of organic
762   matter sources of natural and anthropogenic origins. Applied Geochemistry 31 (0), 239-250.
763 Planquette, H., Sherrell, R.M., 2012. Sampling for particulate trace element determination using water
764   sampling bottles: methodology and comparison to in situ pumps. Limnology and Oceanography:
765   Methods 10 (5), 367-388.
766 Pohl, C., Löffler, A., Hennings, U., 2004. A sediment trap flux study for trace metals under seasonal
767   aspects in the stratified Baltic Sea (Gotland Basin; 57 19.20′ N; 20 03.00′ E). Marine Chemistry 84
768   (3), 143-160.
769 Prahl, F.G., Bennett, J.T., Carpenter, R., 1980. The early diagenesis of aliphatic hydrocarbons and
770   organic matter in sedimentary particulates from Dabob Bay, Washington. Geochimica et
771   Cosmochimica Acta 44 (12), 1967-1976.
772 Prouty, N.G., Campbell, P.L., Mienis, F., Duineveld, G., Demopoulos, A.W.J., Ross, S.W., Brooke, S.,
773   2016. Impact of Deepwater Horizon spill on food supply to deep-sea benthos communities.
774   Estuarine, Coastal and Shelf Science 169, 248-264.
775 Puig, P., Canals, M., Company, J.B., Martín, J., Amblas, D., Lastras, G., Palanques, A., Calafat, A.M.,
776   2012. Ploughing the deep sea floor. Nature 489 (7415), 286-289.
777 Puig, P., Palanques, A., Martín, J., 2014. Contemporary sediment-transport processes in submarine
778   canyons. Annual Review of Marine Science 6, 53-77.
779 Pusceddu, A., Dell'Anno, A., Fabiano, M., Danovaro, R., 2009. Quantity and bioavailability of
780   sediment organic matter as signatures of benthic trophic status. Marine Ecology Progress Series
781   375, 41-52.
782 Raymond, P.A., Bauer, J.E., 2001. Use of ^{14}C and ^{14}C natural abundances for evaluating riverine,
783   estuarine, and coastal DOC and POC sources and cycling: a review and synthesis. Organic
784   Geochemistry 32 (4), 469-485.

785 Rex, M.A., Etter, R.J., 2010. Deep-sea Biodiversity: Pattern and Scale. Harvard University Press,
786   Print, Cambridge. 354 pp.
787 Romero-Romero, S., Molina-Ramírez, A., Höfer, J., Duineveld, G., Rumín-Caparrós, A., Sanchez-
788   Vidal, A., Canals, M., Acuña, J.L., 2016. Seasonal pathways of organic matter within the Avilés
789   submarine canyon: Food web implications. Deep Sea Research Part I: Oceanographic Research
790   Papers 117, 1-10.
791 Ryan, J.P., Yoder, J.A., Cornillon, P.C., 1999. Enhanced chlorophyll at the shelfbreak of the Mid-
792   Atlantic Bight and Georges Bank during the spring transition. Limnology and Oceanography 44
793   (1), 1-11.
794 Schaff, T., Levin, L., Blair, N., DeMaster, D., Pope, R., Boehme, S., 1992. Spatial heterogeneity of
795   benthos on the Carolina continental slope: large (100 km)-scale variation. Marine Ecology-
796   Progress Series 88, 143-143.
797 Schlitzer, R., 2016. Ocean Data View. http://odv.awi.de.
798 Soltwedel, T., 2000. Metazoan meiobenthos along continental margins: a review. Progress in
799   Oceanography 46 (1), 59-84.
800 Stuiver, M., Polach, H.A., 1977. Discussion reporting of 14C data. Radiocarbon 19 (3), 355-363.
801 Tesi, T., Miserocchi, S., Goñi, M.A., Langone, L., 2007. Source, transport and fate of terrestrial
802   organic carbon on the western Mediterranean Sea, Gulf of Lions, France. Marine Chemistry 105
803   (1), 101-117.
804 Tesi, T., Puig, P., Palanques, A., Goñi, M.A., 2010. Lateral advection of organic matter in cascading-
805   dominated submarine canyons. Progress in Oceanography 84 (3), 185-203.
806 Tolosa, I., Miquel, J.C., Gasser, B., Raimbault, P., Goyet, C., Claustre, H., 2008. Distribution of lipid
807   biomarkers and carbon isotope fractionation in contrasting trophic environments of the South East
808   Pacific. Biogeosciences 5 (3), 949-968.
809 Vetter, E.W., Dayton, P.K., 1998. Macrofaunal communities within and adjacent to a detritus-rich
810   submarine canyon system. Deep Sea Research Part II: Topical Studies in Oceanography 45 (1), 25-
811   54.
812 Vogel, J.S., Southon, J.R., Nelson, D.E., 1987. Catalyst and binder effects in the use of filamentous
813   graphite for AMS. Nuclear Instruments & Methods in Physics Research Section B-Beam
814   Interactions with Materials and Atoms 29 (1-2), 50-56.
815 Volkman, J.K., 1986. A review of sterol markers for marine and terrigenous organic matter. Organic
816   Geochemistry 9, 83-99.
817 Volkman, J.K., Revill, A.T., Holdsworth, D.G., Fredericks, D., 2008. Organic matter sources in an
818   enclosed coastal inlet assessed using lipid biomarkers and stable isotopes. Organic Geochemistry
819   39 (6), 689-710.
820 Wakeham, S.G., Lee, C., Hedges, J.I., Hernes, P.J., Peterson, M.J., 1997. Molecular indicators of
821   diagenetic status in marine organic matter. Geochimica et Cosmochimica Acta 61 (24), 5363-5369.
822 Wakeham, S.G., Canuel, E.A., 2006. Degradation and preservation of organic matter in marine
823   sediments. In: K., V.J. (Ed.), The Handbook of Environmental Chemistry, Reactions and
824   Processes. Part N: Marine Organic Matter: Biomarkers, Isotopes and DNA. Springer-Verlag,
825   Berlin, pp. 295-321.
826 Wakeham, S.G., McNichol, A.P., 2014. Transfer of organic carbon through marine water columns to
827   sediments - insights from stable and radiocarbon isotopes of lipid biomarkers. Biogeosciences 11
828   (23), 6895-6914.
829 Wangersky, P.J., Moran, S.B., Pett, R.J., Slauernwhite, D.E., Zhou, X., 1989. Biological control of
830   trace metal residence times: an experimental approach. Marine Chemistry 28 (1-3), 215-226.
831 Wei, C.-L., Rowe, G.T., Hubbard, G.F., Scheltema, A.H., Wilson, G.D.F., Petrescu, I., Foster, J.M.,
832   Wicksten, M.K., Chen, M., Davenport, R., 2010. Bathymetric zonation of deep-sea macrofauna in
833   relation to export of surface phytoplankton production. Marine Ecology Progress Series 399, 1-14.

834   Witbaard, R., Duineveld, G.C.A., Van der Weele, J.A., Berghuis, E.M., Reyss, J.P., 2000. The benthic
835   response to the seasonal deposition of phytopigments at the Porcupine Abyssal Plain in the North
836   East Atlantic. Journal of Sea Research 43 (1), 15-31.
837   Xu, Y., Chant, R., Gong, D., Castelao, R., Glenn, S., Schofield, O., 2011. Seasonal variability of
838   chlorophyll a in the Mid-Atlantic Bight. Continental Shelf Research 31 (16), 1640-1650.
839

Figure 1

Figure 2

Figure 3

Figure 4

Nd (µg g^{-1})

La (µg g^{-1})

Al (µg g^{-1})

Fe (µg g^{-1})

Surface turbid zone.

Nepheloid layer

▼ Shallow (NF-2012-138)   ○ Mid-depth (NF-2012-128)   ● Deep (NF-2012-130)   ◆ Slope (NF-2012-149)

Figure 5

Nutrients (µmol L⁻¹)

Temperature (°C)

a. Nitrate

b. Phosphate

c.. Silicate

d. CTD Stn

Depth [m]

Dissolved Oxygen mg L⁻¹

distance (km)

▼ Shallow (NF-2012-036)
○ Mid-depth (NF-2012-040)
● Deep (NF-2012-051)
◆ Deep (NF-2012-073)

Figure 6

a.

b.

c.

d.
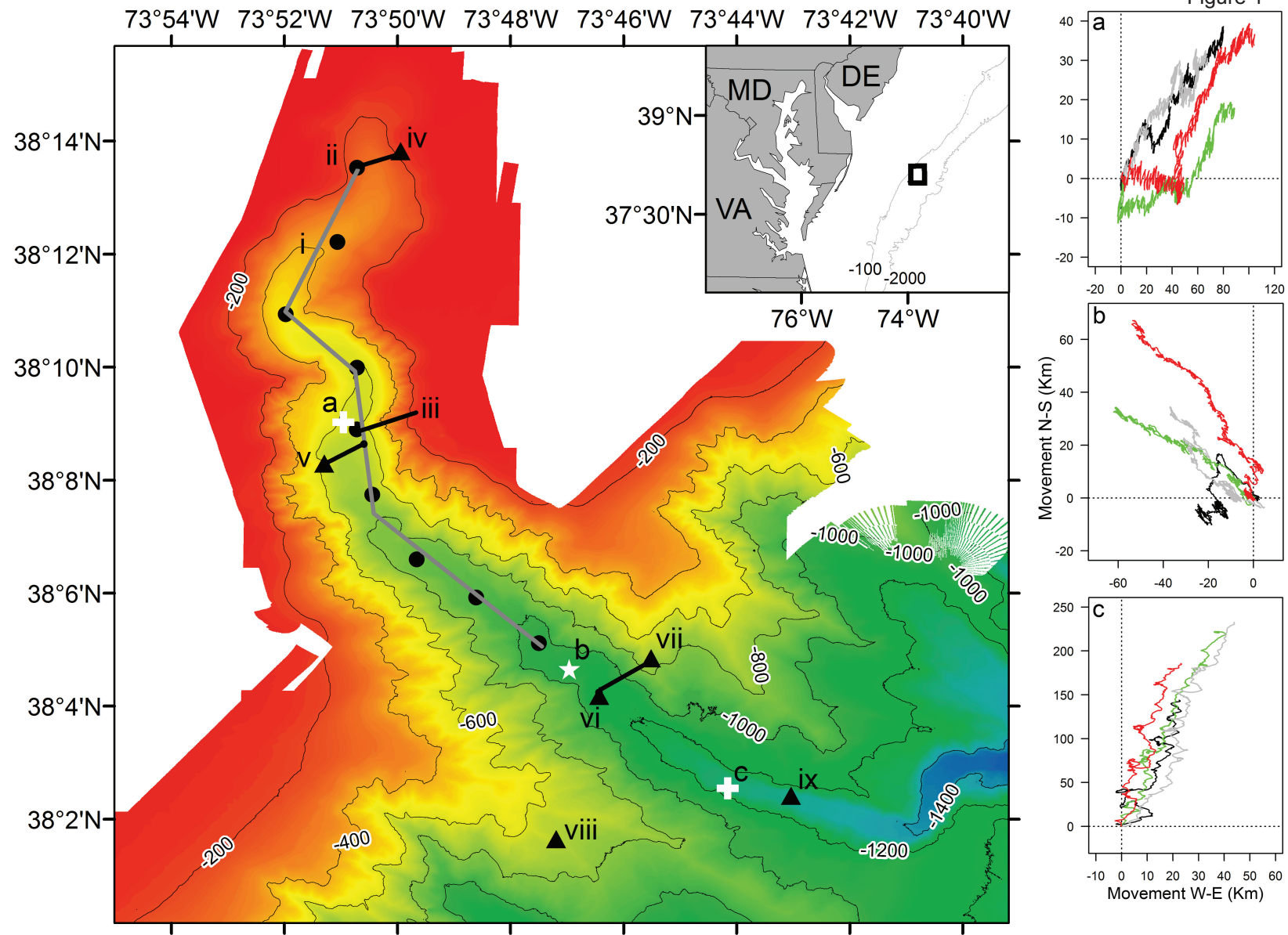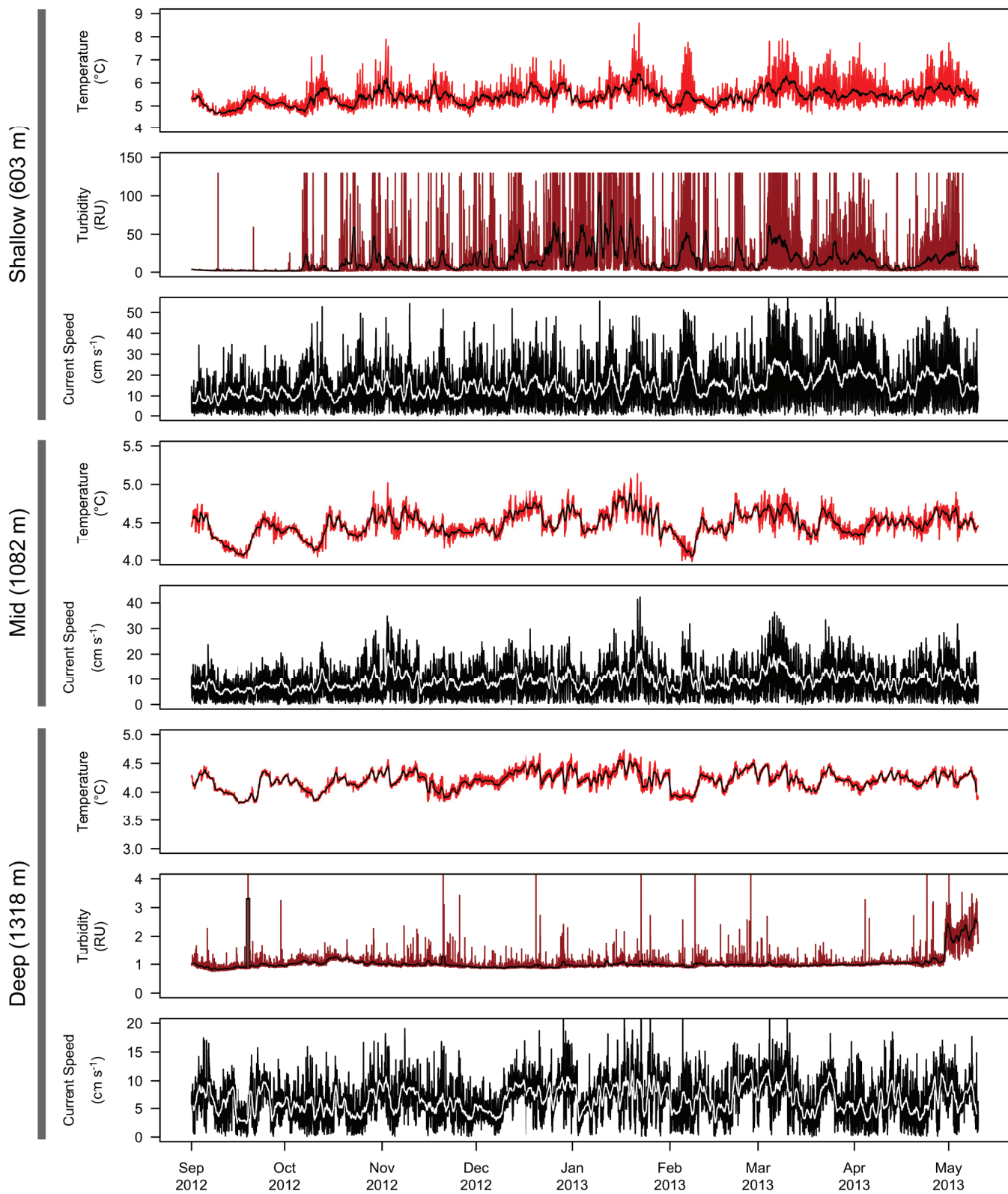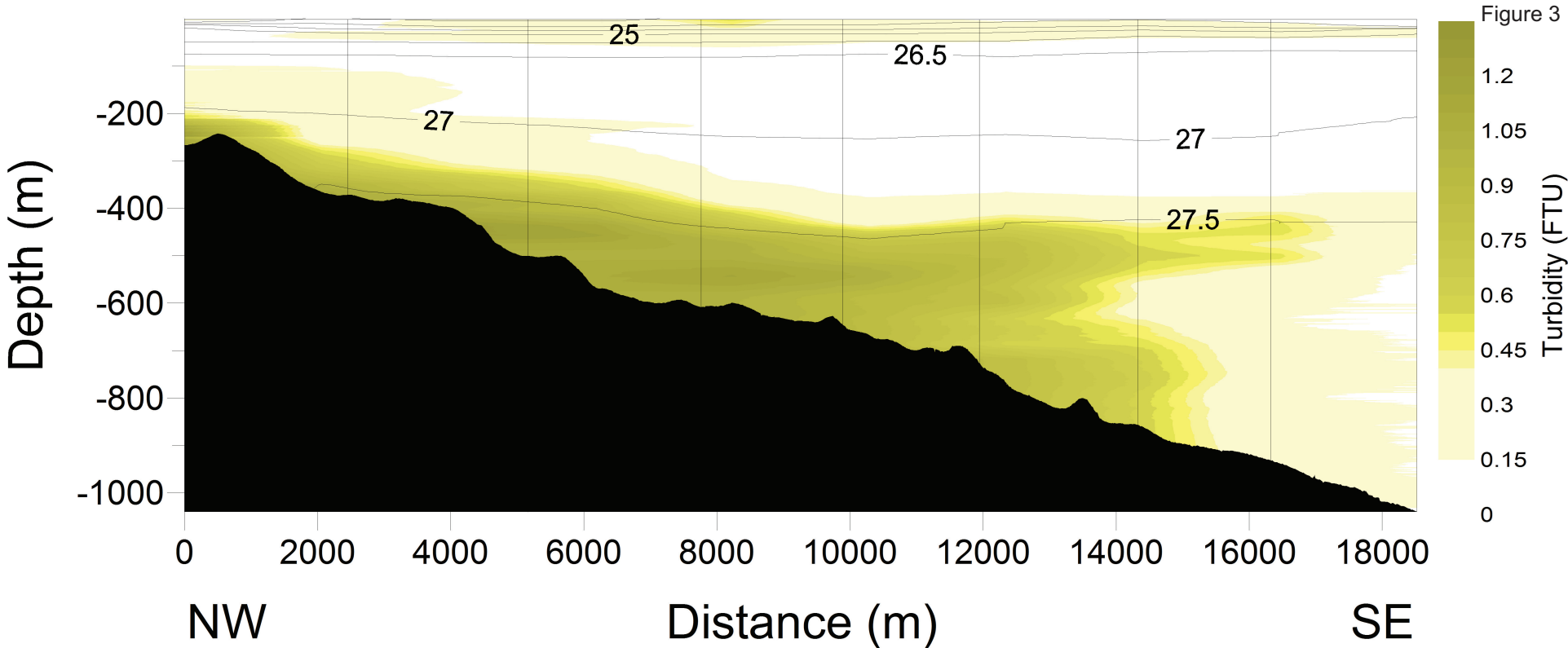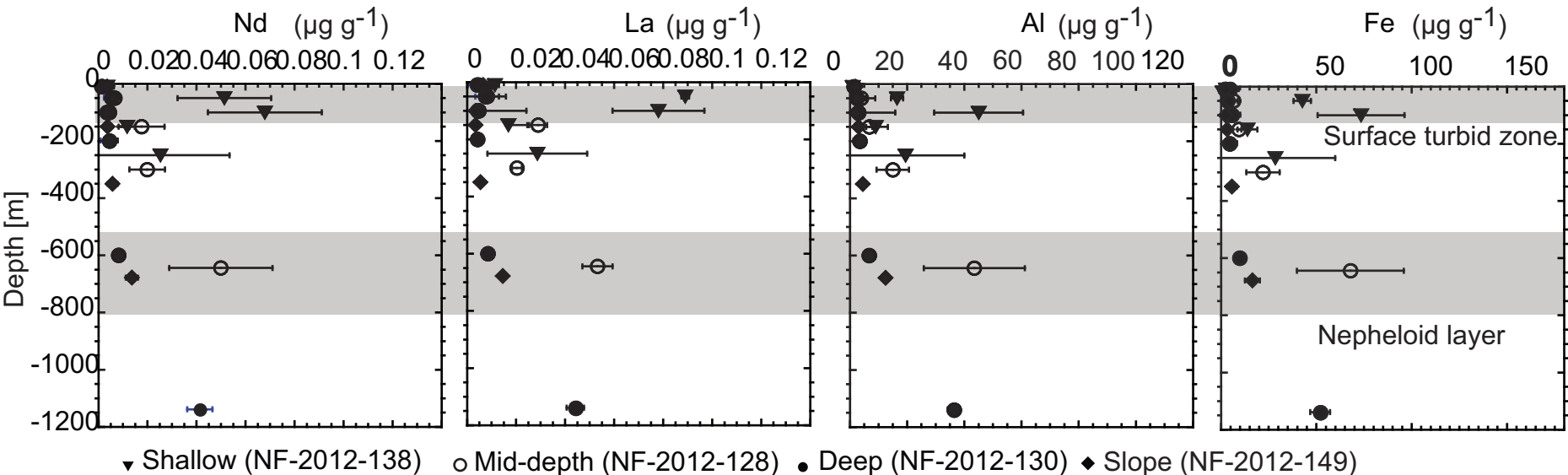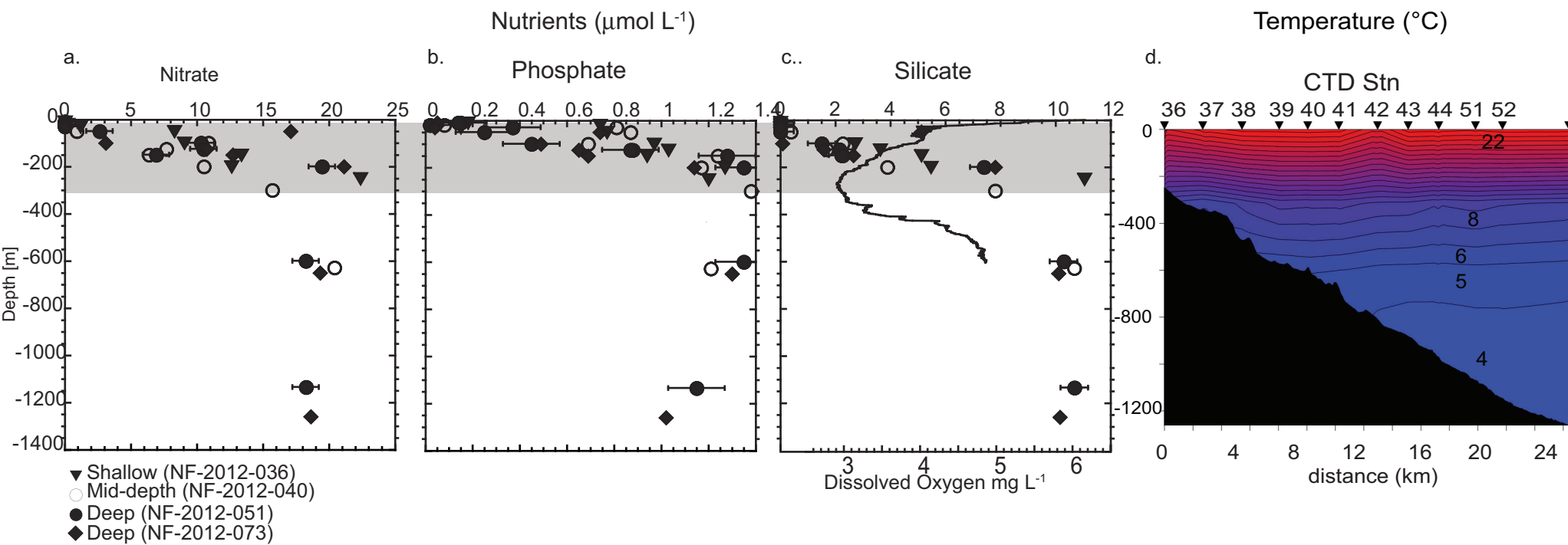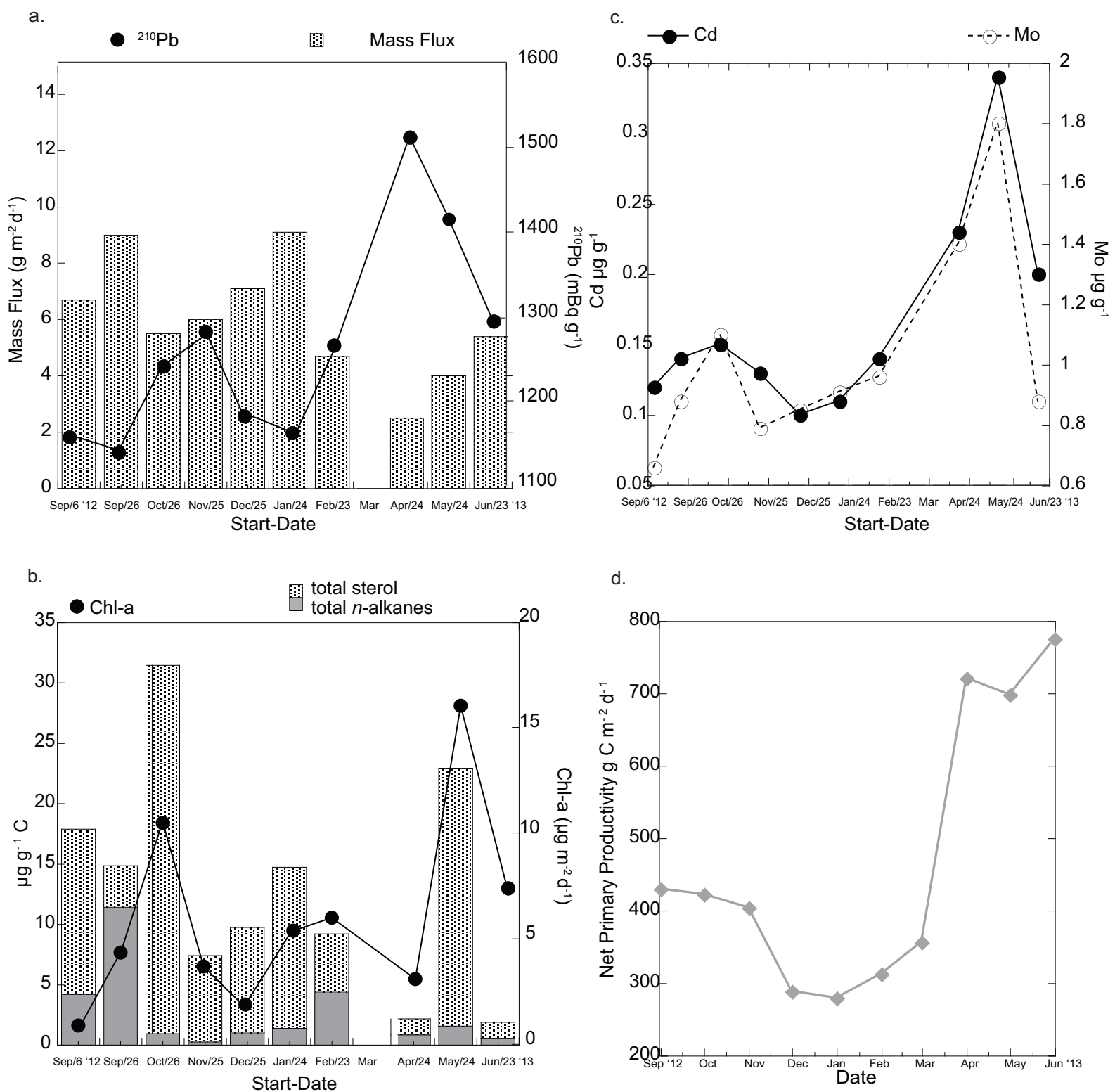
Figure 7
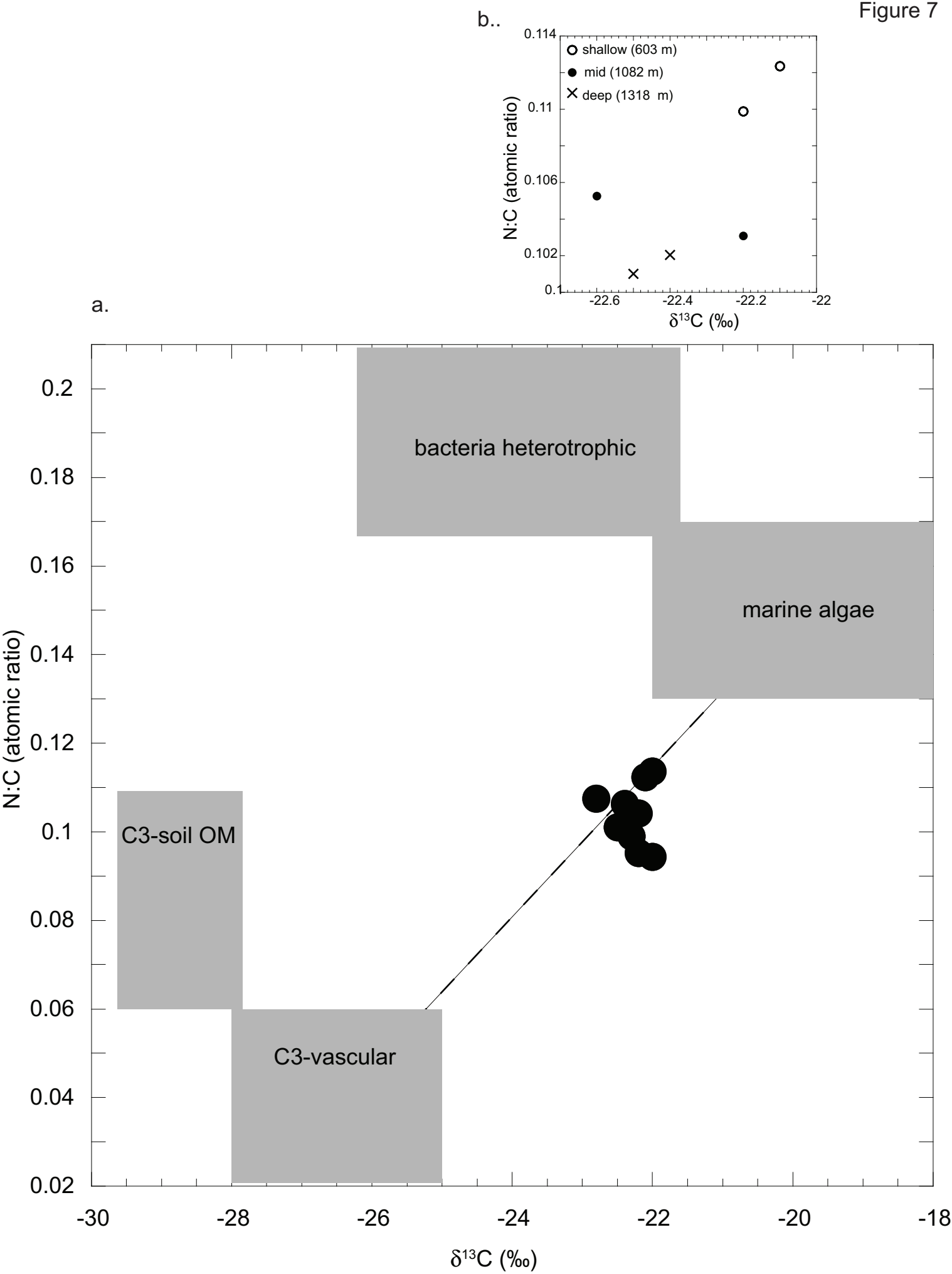
Start-Date	Mass Flux (g m^{-2} d^{-1})	N (%)	$\delta^{15}N$ (‰)	C_{org} (%)	$\delta^{13}C$ (‰)	C:N (atomic)	^{210}Pb (mBq g^{-1})	Chl-a (µg m^{-2} d^{-1})
6-Sep-12	6.7	0.37	5	3.61	-22.4	9.8	1159	0.9
26-Sep-12	9	0.41	5	4.05	-22.5	9.9	1141	4.3
26-Oct-12	5.5	0.41	4.9	3.64	-22.0	8.8	1243	10.5
25-Nov-12	6	0.39	4.9	4.15	-22.0	10.6	1284	3.7
25-Dec-12	7.1	0.39	5	3.74	-22.2	9.6	1184	1.9
24-Jan-13	9.1	0.43	5	3.81	-22.1	8.9	1164	5.4
23-Feb-13	4.7	0.43	4.8	4.32	-22.3	10.1	1268	6
24-Apr-13	2.5	0.41	4.6	4.36	-22.2	10.5	1514	3.1
24-May-13	4	0.42	4.3	3.95	-22.8	9.3	1417	16.1
23-Jun-13	5.4	0.4	4.8	3.75	-22.4	9.4	1296	7.4

Table 1a

Mass fluxes and bulk geochemical measurements from monthly sediment trap samples deployed at 1318 m in Baltimore Canyon, Mid-Atlantic Bight.

Start-Date	Mass Flux (g m^{-2} d^{-1})	N (%)	$\delta^{15}N$ (‰)	C_{org} (%)	$\delta^{13}C$ (‰)	C:N (atomic)	^{210}Pb (mBq g^{-1})	Chl-a (µg m^{-2} d^{-1})
7-Sep-12	16.5	0.39	4.9	3.73	-22.6	9.5	890	n/a
26-Sept-12	52.2	0.38	4.9	3.7	-22.2	9.7	713	n/a

Table 1b

Mass fluxes and bulk geochemical measurements from sediment trap samples deployed at 603 m in Baltimore Canyon, Mid-Atlantic Bight.

Start-Date	Mass Flux (g m^{-2} d^{-1})	N (%)	$\delta^{15}N$ (‰)	C_{org} (%)	$\delta^{13}C$ (‰)	C:N (atomic)	^{210}Pb (mBq g^{-1})	Chl-a (µg m^{-2} d^{-1})
27-Aug-12	4.5	0.42	4.6	3.85	-22.2	9.1	1107	n/a
26-Sept-12	3.9	0.36	4.9	3.21	-22.1	8.9	1115	n/a

Table 1c

Mass fluxes and bulk geochemical measurements from sediment trap samples deployed at 1082 m in Baltimore Canyon, Mid-Atlantic Bight.

Start-Date	n-C_{14}	n-C_{15}	n-C_{16}	n-C_{17}	pr	n-C_{18}	ph	n-C_{19}	n-C_{20}	n-C_{21}	n-C_{22}	n-C_{23}	n-C_{24}	n-C_{25}	n-C_{26}	n-C_{27}	n-C_{28}	n-C_{29}	n-C_{30}	n-C_{31}	n-C_{32}	Σ	CPI	P(aq)
6-Sep-12	n/d	n/d	0.1	n/d	0.09	0.27	0.12	n/d	0.14	0.1	0.16	0.15	0.43	0.36	0.38	0.69	0.46	0.57	0.19	0.19	n/d	4.19	2.42	0.4
26-Sep-12	n/d	0.04	0.03	n/d	n/d	0.08	0.03	n/d	0.04	0.03	n/d	0.06	0.5	0.3	0.7	1.56	1.94	2.55	1.75	1.32	0.53	11.43	5.26	0.09
26-Oct-12	n/d	0.02	0.05	0.03	0.03	0.02	0.07	n/d	0.06	0.04	0.07	0.08	0.07	0.13	0.09	0.15	0.06	0.1	n/d	n/d	n/d	0.97	1.24	0.68
25-Nov-12	n/d	0.02	n/d	0.01	0.01	0.02	n/d	0.03	n/d	0.19	n/d	n/d	n/d	n/d	n/d	n/d	n/d	n/d	n/d	n/d	n/d	0.27	n/a	n/a
25-Dec-12	0.07	0.08	0.06	n/d	n/d	0.05	n/d	n/d	0.04	0.05	n/d	0.07	0.07	0.11	0.06	0.17	n/d	0.2	n/d	n/d	n/d	1.03	2.33	0.47
24-Jan-13	n/d	0.08	0.07	0.04	0.04	0.08	n/d	0.05	0.07	0.06	0.05	0.09	0.07	0.13	0.07	0.18	0.05	0.22	n/d	0.07	n/d	1.38	2.69	0.43
23-Feb-13	0.02	0.06	0.06	0.02	0.03	0.05	n/d	0.03	0.04	0.03	0.05	0.05	3.67	0.08	0.03	0.09	n/d	0.09	n/d	0.04	n/d	4.41	1.63	0.5
24-Apr-13	0.02	0.12	0.1	0.04	0.06	0.07	n/d	0.03	0.08	0.06	0.04	0.05	0.04	0.07	0.01	0.06	0.01	0.07	n/d	n/d	n/d	0.87	1.87	0.63
24-May-13	0.01	0.01	n/d	n/d	0.19	n/d	n/d	0.06	n/d	0.14	0.02	0.21	0.07	0.24	0	0.27	n/d	0.37	n/d	0.19	n/d	1.59	n/a	0.45
23-Jun-13	n/d	n/d	n/d	0.03	0.03	0.02	n/d	0.02	0.01	0.02	0.02	0.06	n/d	0.09	0.02	0.1	0.01	0.1	n/d	0.05	0.01	0.56	7.21	0.5
7-Sept-12[1]	n/d	0.015	n/d	0.014	0.025	0.046	0.013	0.018	n/d	0.022	n/d	0.075	0.166	0.241	n/d	0.255	0.087	0.167	n/d	n/d	n/d	1.11	n/a	n/a
26-Sept-12[1]	n/d	n/d	n/d	n/d	0.026	n/d	n/d	0.048	0.021	0.024	0.034	0.036	0.064	0.042	n/d	0.116	n/d	0.046	n/d	n/d	n/d	0.43	n/a	n/a
27-Aug-12[2]	n/d	0.008	0.004	0.007	0.018	n/d	n/d	0.006	0.009	0.01	n/d	0.025	0.049	0.072	n/d	0.1	0.049	0.06	n/d	n/d	n/d	0.4	n/a	n/a
26-Sept-12[2]	n/d	0.006	0.005	0.008	0.019	0.007	0.008	n/d	0.006	0.009	0.012	0.02	n/d	n/d	n/d	n/d	n/d	n/d	n/d	n/d	n/d	0.07	n/a	n/a

Table 2a

Concentration of total (Σ) and select n-alkane concentrations normalized to organic carbon ($\mu g\ g^{-1}$ C), and parameters including Carbon Preference Index (CPI), and the Alkane Proxy (P_{aq}) in ~monthly sediment trap samples from the deep site (1182 m). Note: *n/d=below detection limit and n/a=calculation not valid due to n/d values*. $P_{aq}=(nC_{23}+nC_{25})/(nC_{23}+nC_{25}+nC_{29}+nC_{31})$ (Ficken et al., 2000); CPI=0.5 * $[(nC_{25} + nC_{27} + nC_{29} + nC_{31})/(nC_{24} + nC_{26} + nC_{28}+ nC_{30})] + [(nC_{25} + nC_{27} + nC_{29} + nC_{31})/(nC_{26} + nC_{28} + nC_{30}+ nC_{32})]$ (Bray and Evans 1961). [1]Data from the shallow (603 m) trap site. [2]Data from the mid-depth (1082 m) trap site. Pr = pristane; ph = phytane

Start -Date	coprostanol	epicoprostanol	5-β-coprostanone	22-dehydrocholesterol	cholesterol	cholestanol	brassicasterol	campesterol	stigmasterol	β-sitosterol	stigmastanol	Σ
6-Sep-12	n/d	n/d	0.72	1.27	3.80	1.21	2.31	0.42	1.10	1.74	1.13	13.71
26-Sep-12	n/d	0.41	0.87	n/d	0.81	n/d	n/d	0.25	0.27	0.83	n/d	3.43
26-Oct-12	n/d	n/d	n/d	3.85	9.02	n/d	6.75	3.61	2.85	3.51	0.89	30.48
25-Nov-12	n/d	n/d	0.34	0.62	2.30	0.57	0.90	0.33	0.71	1.09	0.29	7.16
25-Dec-12	n/d	n/d	0.63	0.67	2.17	0.92	1.10	0.54	1.02	1.31	0.36	8.71
24-Jan-13	n/d	n/d	0.55	6.15	3.01	0.95	2.79	1.05	1.62	2.90	0.58	19.61
23-Feb-13	0.12	0.23	n/d	n/d	0.37	2.36	n/d	0.57	0.27	0.32	0.58	4.82
24-Apr-13	n/d	n/d	0.11	n/d	0.16	0.12	n/d	0.11	0.27	0.20	0.35	1.31
24-May-13	0.13	0.18	0.21	0.94	5.44	8.37	1.44	0.35	1.18	1.52	1.58	21.34
23-Jun-13	n/d	n/d	0.05	n/d	0.28	0.60	0.08	0.10	0.08	0.09	0.07	1.33
7-Sept-12[1]	0.00	0.34	1.15	1.98	10.35	3.30	5.85	2.23	3.46	4.63	2.95	36.23
26-Sept-12[1]	0.05	0.05	0.73	0.30	2.83	1.18	1.84	0.24	0.89	1.48	0.47	10.06
27-Aug-12[2]	0.09	0.00	1.07	0.53	3.99	1.78	2.87	0.38	1.40	2.20	1.46	15.77
26-Sept-12[2]	0.20	0.17	2.05	0.93	7.64	3.40	5.72	0.93	2.99	4.74	2.95	31.73

Table 2b

Concentration of total (Σ) and individual sterols normalized to organic carbon (μg g^{-1} C) in ~monthly sediment trap samples from the deep site (1182 m). Note: *n/d=below detection limit*. [1]Data from the shallow (603 m) trap site. [2]Data from the mid-depth (1082 m) trap site.

Start -Date	%Terrestrial	%Marine	%Anthropogenic
6-Sep-12	40	55	6
26-Sep-12	76	10	14
26-Oct-12	36	63	0
25-Nov-12	35	60	5
25-Dec-12	40	53	7
24-Jan-13	33	64	3
23-Feb-13	38	55	7
24-Apr-13	60	32	8
24-May-13	26	71	3
23-Jun-13	40	55	5
7-Sept-12[1]	37	56	7
26-Sept-12[1]	37	55	8
27-Aug-12[2]	37	59	4
26-Sept-12[2]	31	61	8

Table 3
Major organic matter sources to the sterol and *n*-alkane molecular signatures were investigated by calculating relative proportions of marine, terrestrial higher plants, and anthropogenic/petroleum contributions. Relative contributions from natural (marine versus terrestrial) and anthropogenic organic matter *n*-alkane and sterol sources were calculated following modified designations from Pisani et al. (2013). Terrestrial organic matter composition of sediments was quantified using concentrations of odd-numbered *n*-alkanes in the C_{21} to C_{31} range as well as the sterols campesterol, stigmasterol, β-sitosterol and stigmastanol. Marine components were determined using concentrations of the sterols cholesterol, cholestanol, 22-dehydrocholesterol, and brassicasterol as well as odd- and even-numbered *n*-alkanes in the C_{14} to C_{19} range. The anthropogenic components were determined using the sterol composition of coprostanol, epicoprostanol, and 5-β-coprostanone and the isoprenoid hydrocarbons pristane and phytane.[1]Data from the shallow (603 m) trap site. [2]Data from the mid-depth (1082 m) trap site.

Start -Date	Al	P	V	Cr	Mn	Fe	Cu	Zn	Sr	Mo	Cd	Cs	Ba	La	Tl	Pb	Th	U
6-Sep-12	58200	837	92.9	69.6	538	33600	29.7	91.4	279	0.66	0.12	4.5	449	31.3	0.51	25.9	9.31	2.05
26-Sep-12	56800	870	92	69.4	530	32700	27.5	85.7	283	0.88	0.14	4.5	415	31.3	0.5	28	9.15	2.16
26-Oct-12	55200	886	89.3	66.9	476	31900	28.3	85	298	1.1	0.15	4.4	418	30.4	0.5	26.8	8.84	2.07
25-Nov-12	57300	841	91.6	69.4	648	3 900	28.5	85.4	298	0.79	0.13	4.5	428	32.3	0.51	28.9	9.38	2.18
25-Dec-12	57000	834	91.1	68.3	696	32800	27.9	84.6	285	0.85	0.1	4.5	424	33.4	0.51	28.6	9.65	2.13
24-Jan-13	54200	872	85.2	67.5	568	31700	25	82.8	266	0.91	0.11	4.3	386	31.6	0.48	28	9.23	2.04
23-Feb-13	56200	943	91.6	73.6	501	33100	29.1	88.9	287	0.96	0.14	4.7	422	32.8	0.5	28.4	9.25	2.16
24-Apr-13	55800	948	90.7	68.2	465	32900	30.7	89.7	318	1.4	0.23	4.7	475	32.6	0.52	29.4	9.44	2.26
24-May-13	56800	859	91.4	69.1	440	33600	30.3	86	306	1.8	0.34	4.8	469	33.5	0.53	28.9	9.3	2.18
23-Jun-13	55800	877	90.9	67.4	405	32600	30	82.5	290	0.88	0.2	4.7	466	32.4	0.5	27.1	8.81	2.04
7-Sept-12[1]	54800	858	89.8	68.4	392	32000	26.9	82.4	264	0.97	0.13	4.4	406	33.8	0.49	23.2	9.17	2.23
26-Sept-12[1]	51900	754	82.3	62.3	424	30500	23.4	77.7	274	0.91	0.11	4.2	408	33	0.49	23.4	9.29	2.26
27-Aug-12[2]	55500	809	90.4	66.8	447	32300	27.8	109	277	0.79	0.13	4.6	436	32.1	0.5	24.5	9.29	2.13
26-Sept-12[2]	56600	830	91.5	69.5	439	33000	29.1	83.8	276	0.77	0.16	4.7	438	32.9	0.51	25.5	9.2	2.2

Table 4
Sediment trap trace element concentrations ($\mu g\ g^{-1}$) in ~monthly sediment trap samples from the deep site (1182 m). Al = aluminum; Ba = barium; Cd = cadmium; Cr = chromium; Cs = cesium; Cu = copper; Fe = iron; La = lanthanum; Mn = manganese; Mo = molybdenum; P = phosphorus; Pb = lead; Sr = strontium; Th = thorium; Tl = thallium; U = uranium; V = vanadium; Zn = zinc. [1]Data from the shallow (603 m) trap site. [2]Data from the mid-depth (1082 m) trap site.

Start -Date	Lab ID	F Modern	Fm Err	CRA (years)	CRA error (years)	$\Delta^{14}C$ (‰)	$\Delta^{14}C$ error (‰)	$\delta^{13}C$ (‰)
6-Sep-12	126887	0.8526	0.002	1280	20	-153.75	2.00	-21.68
26-Sep-12	126888	0.8719	0.0018	1100	15	-134.65	1.80	-21.80
26-Oct-12	126889	0.885	0.0019	980	15	-121.57	1.90	-21.58
25-Nov-12	126890	0.8744	0.0018	1080	15	-132.12	1.80	-21.56
25-Dec-12	126891	0.8713	0.002	1110	20	-135.2	2.00	-21.57
24-Jan-13	126892	0.8805	0.0028	1020	25	-126.07	2.80	-21.59
23-Feb-13	126893	0.8754	0.0019	1070	15	-131.13	1.90	-21.73
24-Apr-13	126894	0.8703	0.0019	1120	15	-136.23	1.90	-21.76
24-May-13	126895	0.8758	0.0018	1070	15	-130.77	1.80	-22.15
23-Jun-13	126896	0.8689	0.0024	1130	20	-137.55	2.40	-21.76

Table 5

Radiocarbon results from sediment trap samples from the deep site (1182 m) with fraction modern (Fm) and Fm error (±), with modern defined as 1950, Conventional Radiocarbon Age (CRA) and CRA age error (years), and radiocarbon ($\Delta^{14}C$; ‰) values.

Figure S1

GC-MS total ion chromatogram (TIC) of sediment trap organic matter extracted and fractionated into F1 n-alkane fraction (131-2: 10.20.2012) and F3 sterol and fatty alcohols fraction (131-6: 2.17.2013) extracts. a. aliphatic hydrocarbons, internal standards: 5α androstane b. fatty alcohol/sterol, internal standards: 5α-androstan-3β-ol.

Figure S2

Oceanographic variability in temperature, turbidity and north current speed component for the shallow lander in Baltimore Canyon across two time periods, a. October to November 2012 and b. March to May 2013. Note the mechanism, initially a high turbidity event is followed by approximately 2°C fluctuations in temperature, these spikes are associated with high current speeds.

Station	Sample Type	Depth (m)	%Corg
NF-2012-107	Surface sediment (0−0.5 cm) canyon	283	0.4
NF-2012-114	Surface sediment (0−0.5 cm) canyon	652	0.4
NF-2012-054	Surface sediment (0−0.5 cm) canyon	1180	3.9
NF-2012-065	Surface sediment (0−0.5 cm) slope	170	0.1
NF-2012-070	Surface sediment (0−0.5 cm) slope	515	0.3
NF-2012-084	Surface sediment (0−0.5 cm) slope	990	1.1
NF-2012-091	Surface sediment (0−0.5 cm) slope	1186	1.5

Supplementary Table S1

Surface (0-0.5 cm) sediment samples collected within Baltimore Canyon and adjacent slope and respective percent organic carbon (%Corg).

Sample ID	$n\text{-}C_{14}$	$n\text{-}C_{15}$	$n\text{-}C_{16}$	$n\text{-}C_{17}$	pr	$n\text{-}C_{18}$	ph	$n\text{-}C_{19}$	$n\text{-}C_{20}$	$n\text{-}C_{21}$	$n\text{-}C_{22}$	$n\text{-}C_{23}$	$n\text{-}C_{24}$	$n\text{-}C_{25}$	$n\text{-}C_{26}$	$n\text{-}C_{27}$	$n\text{-}C_{28}$	$n\text{-}C_{29}$	$n\text{-}C_{30}$	$n\text{-}C_{31}$	$n\text{-}C_{32}$	Σ
NF-2012-107	0.49	1.59	0.81	0.78	0.25	1.2	0.44	1.59	1.54	1.32	n/d	0.71	n/d	n/d	n/d	0.61	n/d	0.39	n/d	n/d	n/d	11.03
NF-2012-114	1.96	n/d	3.02	2.65	1.39	2.43	n/d	6.84	4.99	4.79	5.62	13.22	19.32	38.55	44.79	68.61	51.06	71.75	34.55	49.19	14.37	437.71
NF-2012-054	0.12	0.38	0.3	0.43	0.26	0.38	0.32	1.13	0.58	0.63	0.36	0.35	n/d	0.66	0.48	1.08	n/d	0.98	n/d	0.31	n/d	8.19
NF-2012-065	7.38	7.89	4.95	3.9	n/d	4.35	n/d	5.41	5.35	n/d	n/d	n/d	n/d	4.05	n/d	n/d	n/d	n/d	n/d	n/d	n/d	43.28
NF-2012-070	n/d	2.37	2.16	n/d	n/d	2.13	n/d	3.59	3.46	2.67	1.74	n/d	2.41	2.76	n/d	n/d	n/d	n/d	n/d	n/d	n/d	23.29
NF-2012-084	n/d	n/d	13.27	n/d	n/d	18.81	n/d	32.49	30.48	n/d	n/d	n/d	n/d	n/d	n/d	n/d	n/d	n/d	n/d	n/d	n/d	95.04
NF-2012-091	0.34	n/d	1.19	n/d	n/d	1.1	n/d	1.88	n/d	n/d	n/d	n/d	n/d	n/d	n/d	n/d	n/d	n/d	n/d	n/d	n/d	4.51

Supplementary Table S2

Concentration of total (Σ) and select *n*-alkane concentrations normalized to organic carbon ($\mu g\ g^{-1}$ C) in surface (0-0.5 cm) sediment samples in Baltimore Canyon and adjacent slope. Note: *n/d=below detection limit*

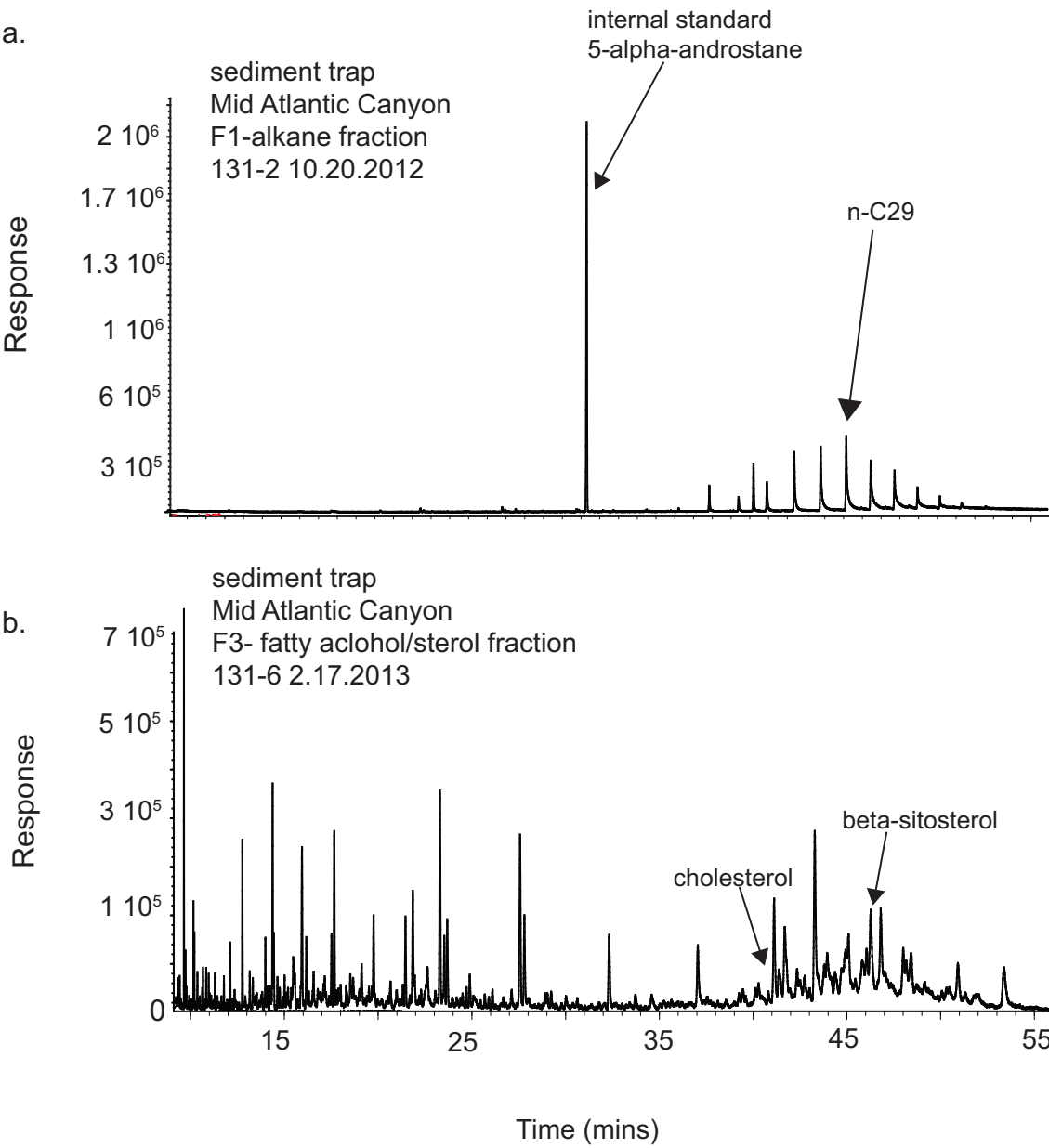| Sample ID	coprostanol	epicoprostanol	5-β-coprostanone	22-dehydrocholesterol	cholesterol	cholestanol	brassicasterol	campesterol	stigmasterol	β-sitosterol	stigmastanol	Σ
NF-2012-107	n/d	n/d	n/d	n/d	1.4	0.76	1.04	3.84	0.75	0.8	0.49	9.08
NF-2012-114	n/d	0.24	n/d	n/d	1.47	2.98	1	2.42	1.21	1.24	n/d	10.56
NF-2012-054	n/d	n/d	n/d	n/d	0.94	0.49	0.87	0.78	0.08	1.26	0.35	4.78
NF-2012-065	n/d	n/d	n/d	n/d	2.6	0.87	n/d	13.1	4.39	1.5	2.13	24.59
NF-2012-070	n/d	n/d	n/d	n/d	2.38	1.21	1.31	2.08	1.36	1.18	1.42	10.95
NF-2012-084	n/d	n/d	n/d	n/d	n/d	n/d	n/d	n/d	n/d	n/d	n/d	n/d
NF-2012-091	n/d	n/d	n/d	n/d	n/d	n/d	n/d	n/d	n/d	n/d	n/d	n/d

Supplementary Table S3

Concentration of total (Σ) and individual sterols normalized to organic carbon (μg g^{-1} C) in surface (0-0.5 cm) sediment samples in Baltimore Canyon and adjacent slope. Note: *n/d=below detection limit*
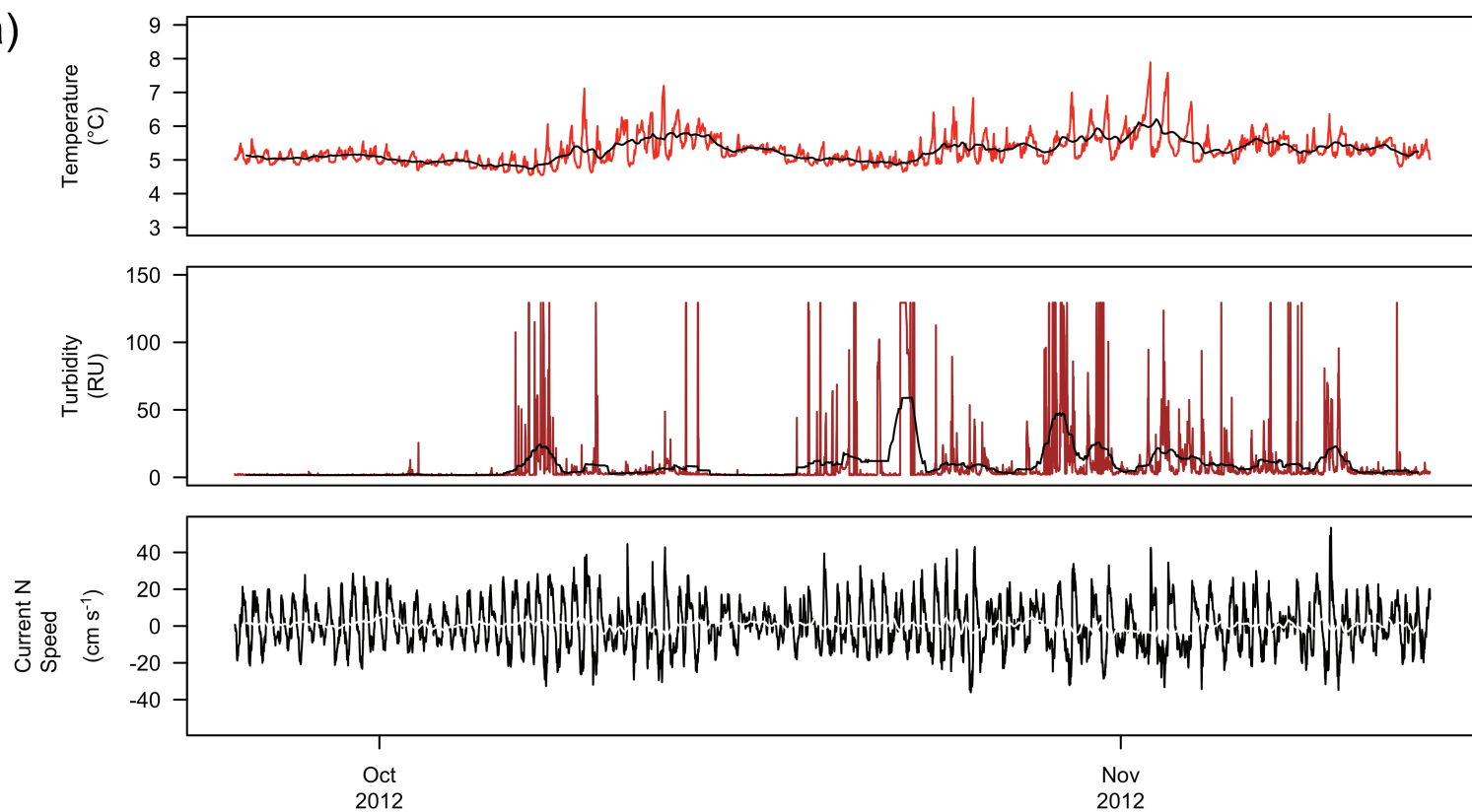
Site	%Terrestrial	%Marine	%Anthropogenic
NF-2012-107	46	50	4
NF-2012-114	91	8	1
NF-2012-054	54	42	5
NF-2012-065	40	60	0
NF-2012-070	43	57	0
NF-2012-084	n/a	n/a	n/a
NF-2012-091	n/a	n/a	n/a

Supplementary Table S4

Major organic matter sources to the sterol and *n*-alkane molecular signatures were investigated by calculating relative proportions of marine, terrestrial higher plants, and anthropogenic/petroleum contributions in surface sediment samples in Baltimore Canyon and adjacent slope. Relative contributions from natural (marine versus terrestrial) and anthropogenic organic matter *n*-alkane and sterol sources were calculated following modified designations from Pisani et al. (2013). Terrestrial organic matter composition of sediments was quantified using concentrations of odd-numbered *n*-alkanes in the C_{21} to C_{31} range as well as the sterols campesterol, stigmasterol, β-sitosterol and stigmastanol. Marine components were determined using concentrations of the sterols cholesterol, cholestanol, 22-dehydrocholesterol, and brassicasterol as well as odd- and even-numbered *n*-alkanes in the C_{14} to C_{19} range. The anthropogenic components were determined using the sterol composition of coprostanol, epicoprostanol, and 5-β-coprostanone and the isoprenoid hydrocarbons pristane and phytane. *Note: n/a=Source contributions were not calculated due to non-detect sterol and select n-alkane concentrations (Table S2).*